THE BOUNDARY LAYERS OF THE ATMOSPHERE AND OCEAN

N.A.T.O. Advanced Study Institute

Ramsey, Isle of Man

21 Sept. to 2 Oct. 1970

Report by

E. C. Nickerson

Sponsored by

Office of Naval Research

Contract No. N0014-68-A-0493-0001

Project No. NR062-414/6-6-68 (Code 438)

U. S. Department of Defense

Washington, D. C.

ID70-71-3

TABLE OF CONTENTS

* Recording available - fair quality
*+ Recording available - good quality
*- Recording available - poor quality
** Part of recording available
*** Tape jams

Introduction

A N.A.T.O advanced study institute was held at Ramsey, Isle of Man. The institute consisted of lectures and discussions on various aspects of the atmospheric and oceanic boundary layers and of air-sea interaction. Emphasis was primarily on the way in which boundary layer processes affect the larger-scale motions of the atmosphere and ocean. A unique advantage which this type of scientific gathering enjoys over a more conventional conference is the time allowed for informal discussions and additional unscheduled seminars.

The purpose of the meeting was to shorten the gap between training and individual research. Lecturers assumed a basic knowledge of physics and applied mathematics in the context of meteorological and oceanographic phenomena.

This report should not be construed as representing the proceedings of the Advanced Study Institute. Sections of particular interest to the author are reported on in much more detail than sections of less interest. Lectures on the fundamentals of gravity waves or radiation theory, for example, which are in many standard texts, are only briefly discussed. Also, some lectures consisted primarily of slides or movies with few resultant notes.

The author recorded most of the lectures on a small portable cassette tape recorder. Approximately half of these tapes are of a quality to warrant listening to. The tapes are available to interested parties on a short term loan basis.

CHARNOCK - Introduction, problems, and methods of attack

The primary aim of the conference is to focus on the upper portion of the atmospheric boundary layer and the lower portion of the oceanic boundary layer in order to examine the connecting links between the free atmosphere and the free ocean. The lowest hundred meters of the atmosphere best correspond to a laboratory channel and may be termed a "happy hunting ground" for experimentalists. Motions on a scale comparable to the height of the boundary layer must be taken into account in a realistic large scale numerical model. Also, since most of the energy from the sun is absorbed in the top few meters of the ocean, any long term numerical model must realistically take into account this energy source.

ROLL - Boundary layer over the sea

Very close to the sea surface there exists an interfacial layer in which molecular processes are dominant and where the exchange of heat occurs. However, under strong wind conditions the sea surface may be ill-defined. A high concentration of carbon monoxide exists at the sea surface leading to a flux of CO into the atmosphere from the ocean.

Hydrodynamic anology. Suppose we consider a two dimensional flow over a solid boundary. An upper turbulent region is separated from the laminar region next to the boundary by a transition region. The top of the laminar layer occurs at a height of ν/u_*, while the top of the transition layer occurs at a height of approximately $30\ \nu/u_*$. Here ν is the kinematic viscosity and u_* the friction velocity. If a Reynolds number is defined by $h\ u_*/\nu$, where h is the height of the physical obstacles which comprise the boundary, the surface is

said to be aerodynamically smooth for Reynolds number much less than unity, and aerodynamically rough for Reynolds numbers much larger than unity. The mean velocity profile in the smooth case is given by

$$U = \frac{u_*}{k} \ln\left(\frac{9.1\, u_* z}{\nu}\right), \tag{1}$$

and by

$$U = \frac{u_*}{k} \ln\left(\frac{z}{z_o}\right) \tag{2}$$

for the rough boundary. In hydraulics, z_o corresponds to h/30.

Vertical wind profile. The log profile in general is verified over the sea surface for neutrally stratified conditions. Kinks which have been observed at various heights in the log profile are apparently due to non-stationarity. One hour averages are occasionally needed to obtain steady profiles.

Aerodynamic roughness over sea surface. Significant differences exist between the observations of various investigators. One result which seems to stand out, however, is that the drag at the sea surface appears to be less than that over a smooth wall. This is somewhat paradoxical since one often associates an increased drag with a roughened surface. It has been shown quite conclusively, moreover, that the nature of the rough surface over the sea is not equivalent to that over a rigid rough surface.

Various attempts have been made to find expressions for the surface roughness in terms of relevant physical parameters. An example of this search for functional relationships occurs in the work of Zilitinkevich (1969), who proposes the general relation:

$$z_o = \frac{u_*^2}{g} f\left(\frac{u_* z}{g \nu}\right) . \qquad (3)$$

For a smooth surface, $f = g\nu/u_*^3$, which leads to z_o proportional to ν/u_*. For a rough surface, on the other hand, f is a constant, which leads to z_o proportional to u_*^2/g.

Ruggles (1969) observed peaks in the values of z_o when plotted against the mean wind speed at ten meters. A schematic diagram appears below.

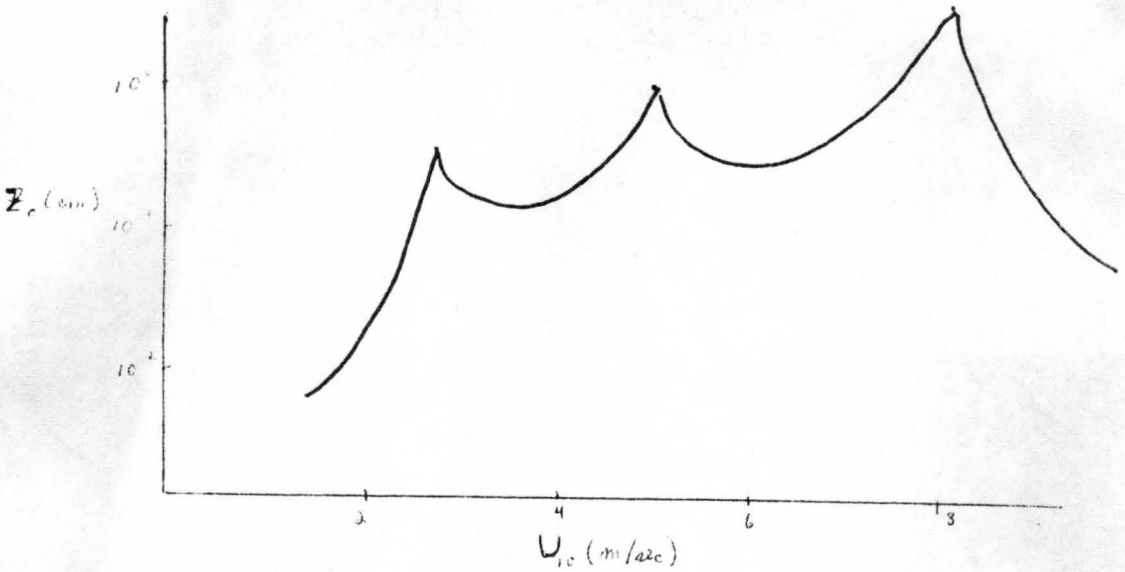

The peaks in z_o indicate the possible existence of critical wind speeds. A list of references is included at the end of this report.

DORRESTEIN - Gravity wave theory (see abstract)

A lecture on the fundamentals of gravity wave theory was presented. The Gerstner and Stokes waves were examined in some detail, particularly with regard to their mass transports in both Eulerian and Lagrangian frames of reference.

wave travel to right →

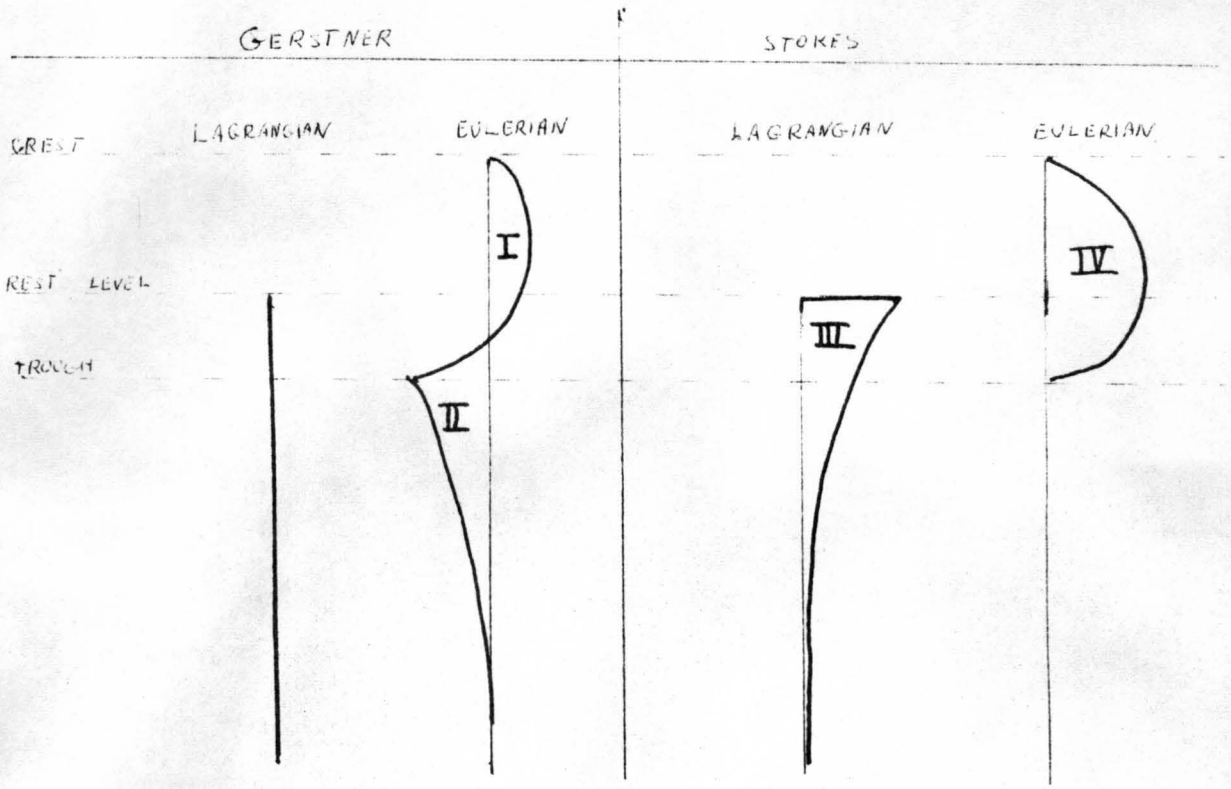

Area I = Area II

Area III = Area IV

A handout pertaining to gravity waves is to be found at the end of this report.

CHARNOCK - Similarity theory

The separation of the velocity field into mean and fluctuating quantities is a standard procedure in the study of turbulent motions. Yet an averaging process of the form $\overline{U} = 1/T \int_0^T U dt$ does not satisfy the conditions $\overline{\overline{U}} = \overline{U}$, $\overline{U'} = 0$, $\overline{\partial U}/\partial z = \partial \overline{U}/\partial z$, $\overline{\overline{U}\,\overline{U}} = \overline{U}\,\overline{U}$, $\overline{\overline{U}\,U'} = 0$.

Laboratory data indicate the following sort of relationship between surface roughness and obstacle height.

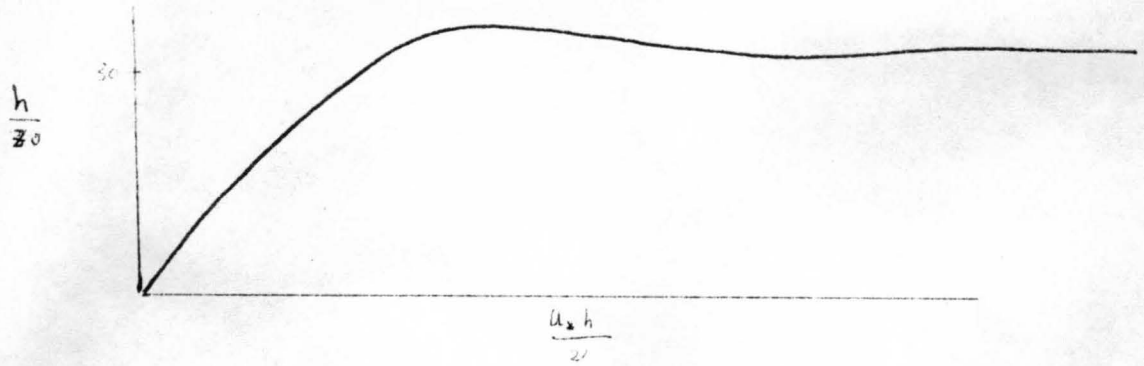

Measurements of shearing stress on the sea surface have been computed by measuring the tilt of the sea surface, that is, by assuming a balance of the form

$$\frac{\partial P}{\partial x} = \frac{\partial \tau}{\partial z} \quad , \tag{4}$$

which leads to $\tau_o = \rho g d$. A necessary requirement for this relation to be of some use is for a steady state condition to exist. It is then suggested that

$$g z_c \rho_{water} = \rho_{air} u_*^2 \quad , \tag{5}$$

which leads to a roughness height proportional to u_*^2/g.

JERLOV - Radiation processes

Absorption of radiation by water is the primary phenomenon to be considered (other effects are of considerably less importance). Sea surface processes that alter the absorption process include direct and diffuse reflection.

Energy penetration is increased for a roughened sea surface and decreased for a smooth surface.

ROLL - Boundary layer over the sea continued

Roughness lengths corresponding to flow over water have been obtained both in the field and in the laboratory. Iwata (1969) found that the Charnock relation did not hold (i.e. gz_o/u_*^2 was not a constant), but that z_o depended on the quantities $u_*^3/g\nu$ and gH/u_*^2, where H is the wave height. Hidy and Plate (1967) found z_o proportional to u_*H/ν. Wu (1968) found that below a critical wind speed of 8.2 m/sec, $z_o = .18T/\rho u_*^2$, where T is the surface tension. (Roll did not remember the height to which the critical speed referred). A definite trend was observed by Wu in the laboratory experiments between z_o and the number of ripples on the gravity waves. If $u > 8.2$ m/sec, $z_o = .0112\, u_*^2/g$. Here the roughness is in some way governed by gravity waves.

A theoretical study by Kraus (1966) predicted flow separation when the mean velocity in the laminar sub-layer exceeded the velocity of the slowest waves. The mean velocity in the sub-layer was given by $u = u_*/2k$, which leads to the separation criteria of $u_* > 2k\, c_o$ (where c_o = speed of the slowest waves), or a value of approximately 18 cm/sec for a Stokes wave.

A primary cause of wave growth is the normal pressure at the sea surface. The fact that surface waves are nearly irrotational gives credence to the importance of normal pressure fluctuations.

The tangential stress at the sea surface may be expressed in terms of the wind speed at 10 meters by the relation

$$\tau_o = \rho C_{10} \left(\bar{U}_{10}^2 - U_s^2 \right) , \qquad (6)$$

where u_s is the surface speed.

$$C_{10} = \left(\frac{u_*}{\bar{U}_{10}}\right)^2 = \frac{k^2}{\left(\ln \frac{10}{z_0}\right)^2} \qquad (7)$$

Observations prior to 1964 lead to the following picture.

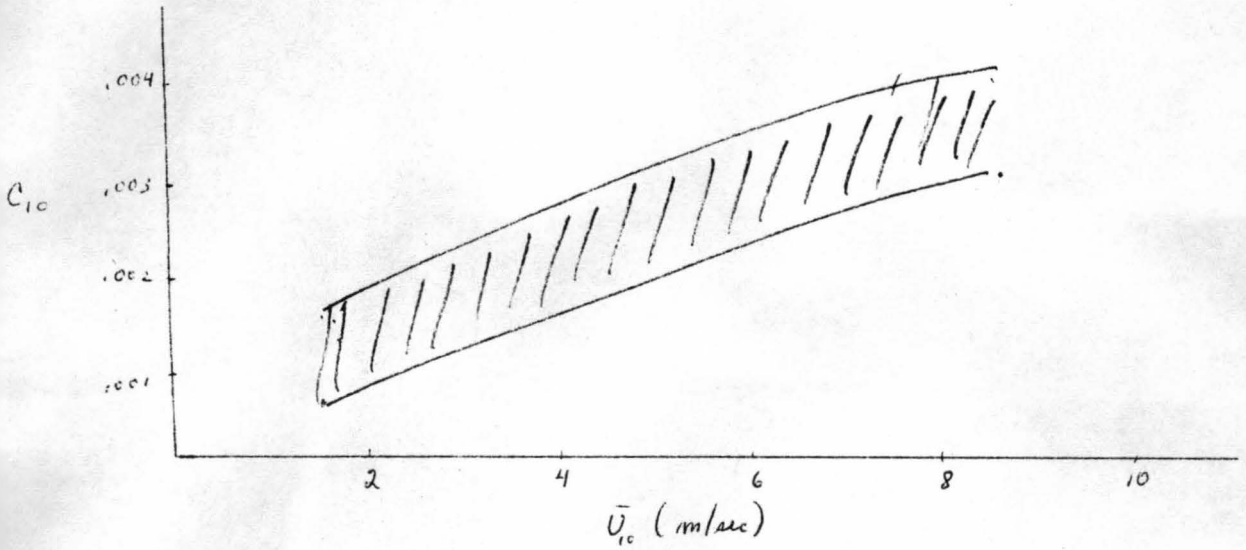

The observations of Ruggles (1969) are indicated below.

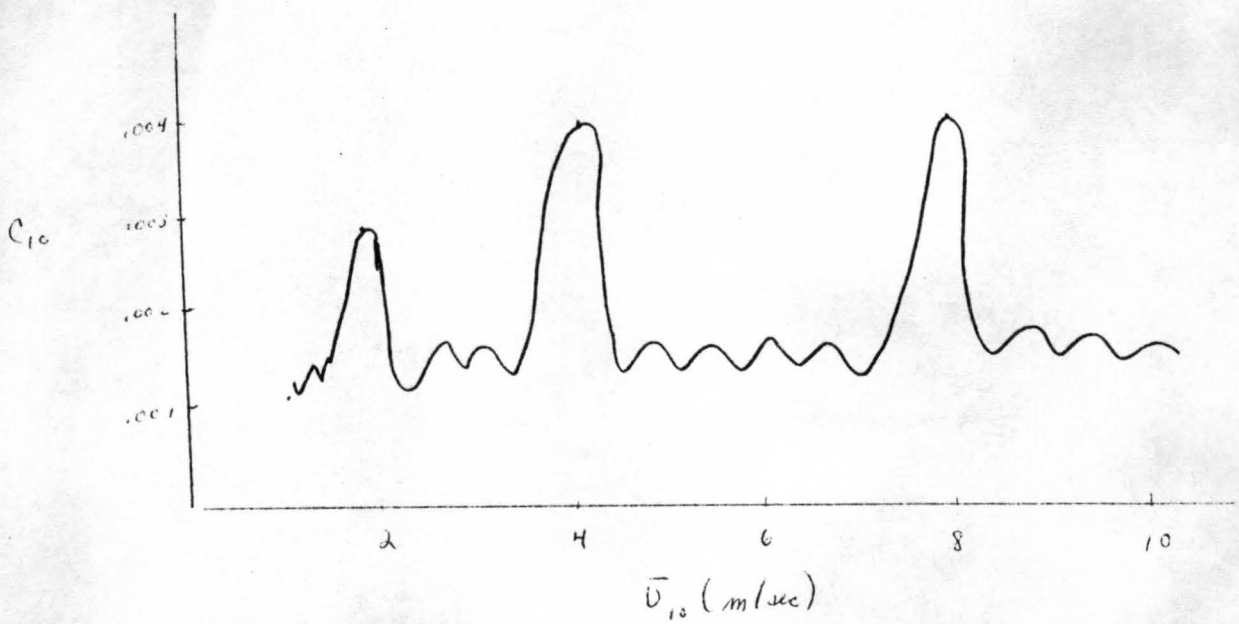

Wu's results show the following.

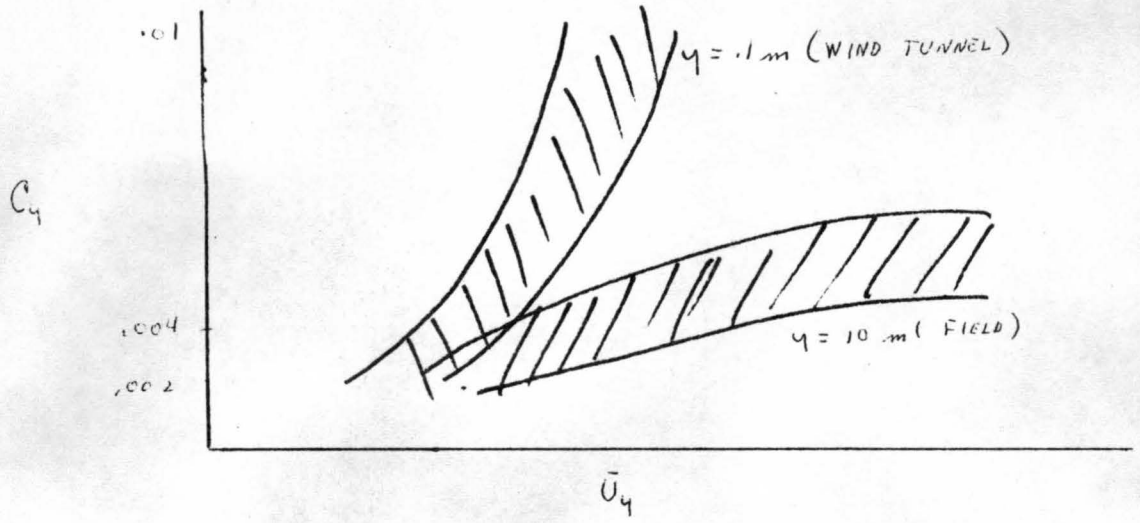

The status of the composite picture at this point of the various results is not satisfactory, and it is suggested that any attempt to group the data should take into account the density stratification. The qualitative effects of density stratifications on the wind profile are indicated below.

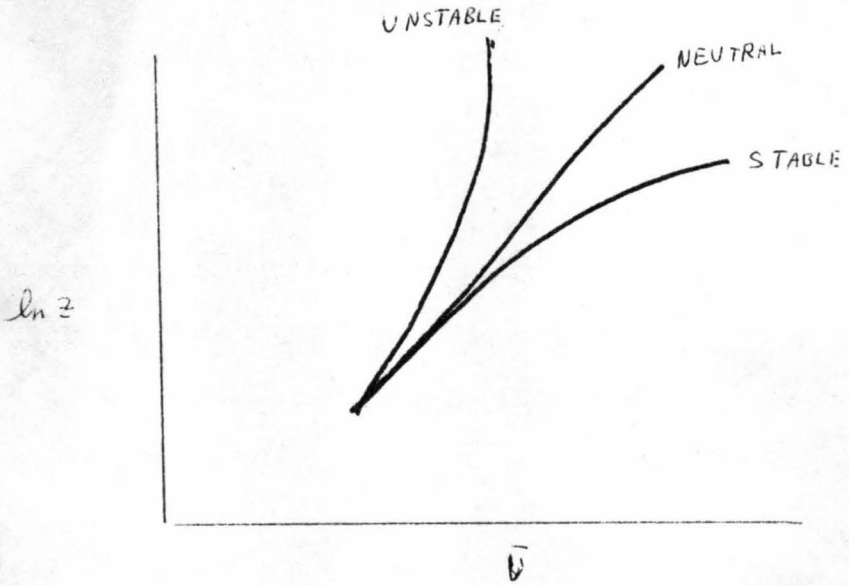

The definition of flux Richardson number must include the flux of latent as well as sensible heat. This is particularly important in the tropics. Similarly, the gradient Richardson number should be expressed in terms of the virtual temperature.

$$R_f = \frac{-g}{\bar{T}\frac{\partial \bar{U}}{\partial z}}\left(\frac{H}{C_p \bar{T}} + r\bar{E}\right) \tag{8}$$

$$\bar{E} = -\rho K_E \frac{\partial \bar{q}}{\partial z} \tag{9}$$

$$H = -\rho C_p K_H \frac{\partial \theta}{\partial z} \tag{10}$$

$$R_{i_v} = \frac{\frac{g}{\bar{T}_v}\frac{\partial \theta_v}{\partial z}}{\left(\frac{\partial \bar{u}}{\partial z}\right)^2} \tag{11}$$

$$R_f = \frac{K_H}{K_M} R_{i_v} \tag{12}$$

$$\frac{\partial \bar{U}}{\partial z} = \frac{u_*}{kz} S(R_f) \tag{13}$$

$$L_v = \frac{-\rho u_*^3}{gk\left(\frac{H}{C_p \bar{T}} + r\bar{E}\right)} \quad , r = 0.6 \tag{14}$$

$$\frac{z}{L_v} = \frac{K_H}{K_m} R_{i_v} \zeta \quad . \tag{15}$$

For unstable conditions, Ellison proposed

$$\zeta = \left(1 - \frac{\gamma K_H}{K_m} R_{i_v}\right)^{-1/4} . \tag{16}$$

For stable conditions, Monin and Obukhov proposed

$$\zeta = 1 + \frac{\alpha z}{L_v} = \left(1 - \frac{\alpha K_H}{K_m} R_{i_v}\right)^{-1} \tag{17}$$

$$U = \frac{u_*}{k} \left[\ln\left(\frac{z}{z_0}\right) - \psi\left(R_{i_v}\right) \right] . \tag{18}$$

Brocks and Krugermeyer (1970) have examined the drag coefficient in terms of the Richardson number. If one applied the log profile in the usual form without regard to stability, one would have an apparent friction velocity given by

$$"u_*" = \zeta u_* \tag{19}$$

$$\log "z_0" = \log z - \frac{1}{\zeta}\left(\log \frac{z}{z_0} - \psi\right) . \tag{20}$$

For values of $\gamma \frac{K_H}{K_M} = 18$, and $\alpha \frac{K_H}{K_M} = 4.5$, the errors are as follows.

"u_*"/u_*	Ri_v
.77	-.01
1.8	+.01

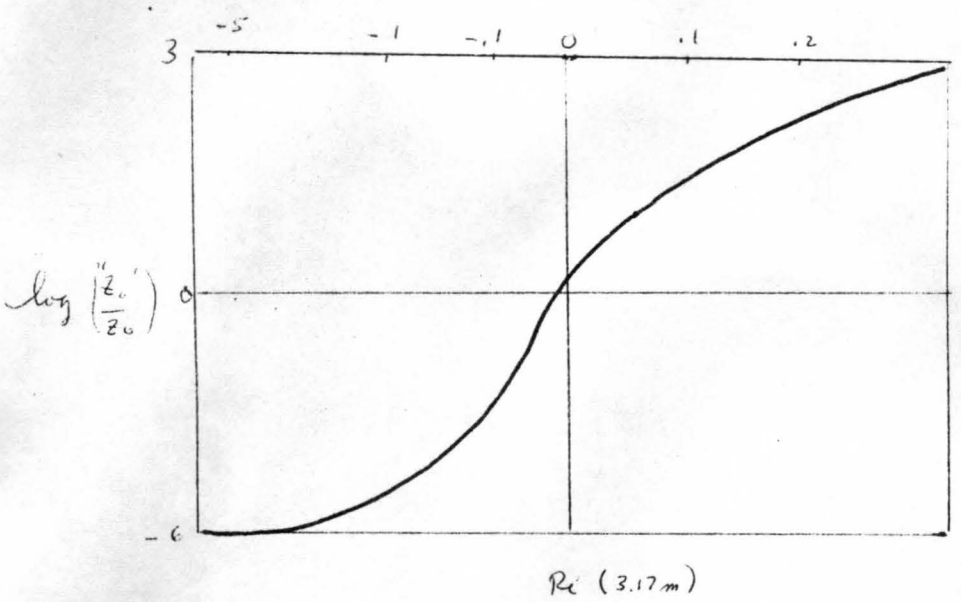

The errors in the computation of z_o are seen to be even more serious than in the computation of u_*

For $|Ri_v| \leq .1$, Brocks and Krugermeyer obtain the following results from a large number of profiles.

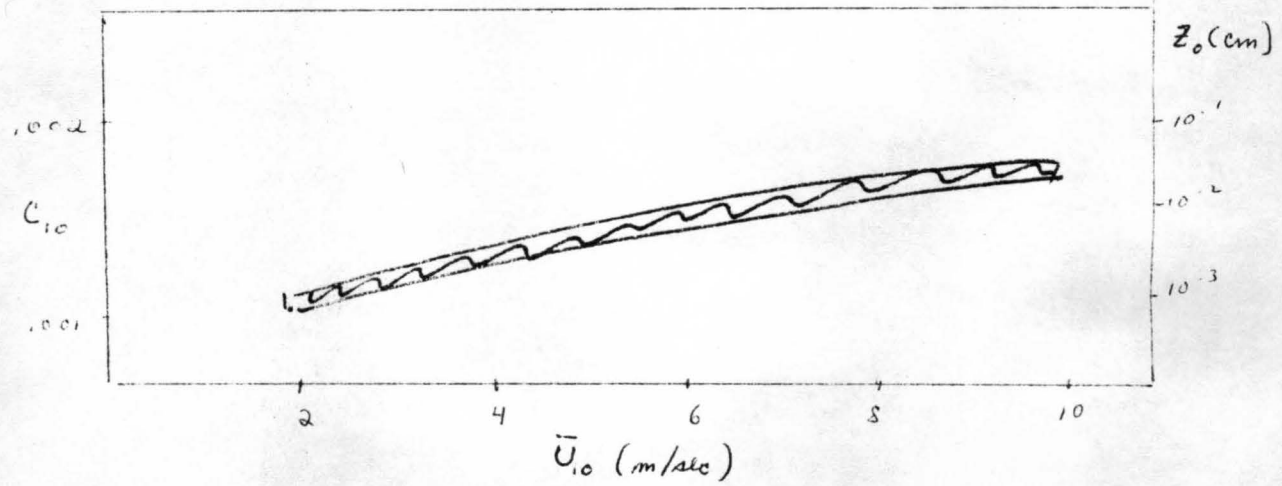

A representative value of c_{10} is .0013. Independent values for different areas are the following.

Baltic Sea	$c_{10} = (1.36 \pm .21) \times 10^{-3}$
North Sea	$c_{10} = (1.25 \pm .14) \times 10^{-3}$
North Atlantic	$c_{10} = (1.30 \pm .18) \times 10^{-3}$

In the Baltic and North Sea, $z_o = 1.5 \times 10^{-2}$ cm.

The primary conclusion then is that the wind profile method is satisfactory if you take into account the stratification.

CHARNOCK - Similarity theory continued

We are now at the point where we are arguing over a factor of two for the value of the drag coefficient over the sea. If one were faced with the task of estimating the stress, the largest source of error would probably occur in the evaluation of the wind speed.

Let us now examine the transfer of scalar quantities in the constant flux layer.

$$\theta_* = \frac{\langle w\theta \rangle}{u_*} \tag{21}$$

$$q_* = \frac{\langle wq \rangle}{u_*} \tag{22}$$

$$\frac{kz}{\theta_*} \frac{\partial \theta}{\partial z} = \frac{1}{\alpha_\theta} \tag{23}$$

$$\frac{kz}{q_*} \frac{\partial q}{\partial z} = \frac{1}{\alpha_q} \tag{24}$$

In the last relation we have assumed dynamic similarity between heat and moisture. The value of α_o appears to be slightly larger than unity (1.1 to 1.3). Conditions at the surface come in as boundary conditions.

$$\frac{\theta - \theta_s}{\theta_*} = \frac{1}{\alpha_o k} \ln \frac{z}{z_\theta(0)} \quad . \tag{25}$$

The meaning of $z_\theta(0)$ and $z_q(0)$ are not very clear, especially over land. There is even an argument as to what we mean by the surface temperature of the sea.

Above the surface layer, the Coriolis parameter becomes important.

$$u - u_g = u_* F_1 \left(\frac{fz}{u_*} \right) \tag{26}$$

$$v - v_g = u_* F_2 \left(\frac{fz}{u_*} \right) \tag{27}$$

Near the surface we have the log law

$$F_1 = \ln \left(\frac{fz}{u_*} \right) + A \tag{28}$$

$$F_2 = \frac{1}{k} B \tag{29}$$

where A and B are constants, and f is the Coriolis parameter.

$$k \frac{u_g}{u_*} = \ln \left(\frac{u_*}{f z_o} \right) - A \tag{30}$$

$$\frac{k v_g}{u_*} = -B \tag{31}$$

These neutral Ekman layer relations are of not much use since we have assumed steady state conditions, horizontal homogeneity, and neutral conditions throughout the layer. It would be very dangerous to attempt to estimate the stress at the sea surface using ageostrophic arguments.

The existence of a mean density gradient has a significant effect on turbulent transport processes. In unstable conditions for fixed shearing stress, the turbulence would be stronger than in the neutral case.

$$E = \frac{1}{2}\left(u^2 + v^2 + w^2\right) \tag{32}$$

$$\frac{\partial E}{\partial t} = u_*^2 \frac{\partial U}{\partial z} + \langle w'\rho' \rangle \frac{g}{\rho} - \varepsilon - D \,, \tag{33}$$

where D = divergence term, ε = dissipation term. After normalizing the energy equation, we obtain:

$$\frac{kz}{u_*^3} \frac{\partial E}{\partial t} = \phi_M - \phi_\varepsilon - \phi_D - \zeta \,. \tag{34}$$

We now make the following definitions and assume that any non-dimensional part of the turbulence must depend only upon ζ.

$$\phi_m = \frac{kz}{u_*} \frac{\partial U}{\partial z} = \phi_M(\zeta) \tag{35}$$

$$\phi_H = \frac{kz}{\theta_*}\frac{\partial\theta}{\partial z} = \phi_H(\zeta) \tag{36}$$

$$\zeta = \frac{kz}{u_*^3}\langle w'\rho'\rangle\frac{g}{\rho} = \frac{z}{L} \tag{37}$$

$$\phi_v = \frac{kz}{q_*}\frac{\partial q}{\partial z} = \phi_H \tag{38}$$

$$\phi_m(0) = 1 \tag{39}$$

$$\phi_H(0) = \frac{1}{\alpha_0} \tag{40}$$

Either ζ, R_f or Ri may be used as a profile parameter.

$$R_f = \frac{\zeta}{\phi_m} = \alpha R_i \tag{41}$$

$$\alpha = \frac{\phi_M}{\phi_H} \tag{42}$$

Direct measurement seems to be the best way to measure fluxes.

For stable conditions, the Russians proposed the log-linear profile.

$$\frac{kU}{u_*} = \ln\left(\frac{z}{z_0}\right) + \alpha\frac{z}{L} \tag{43}$$

where $\alpha = .6$. The Australians, however, analyzed their data in terms of that law and found a good fit provided $\alpha = 5$, which is nearly an order of magnitude larger than the Russian value.

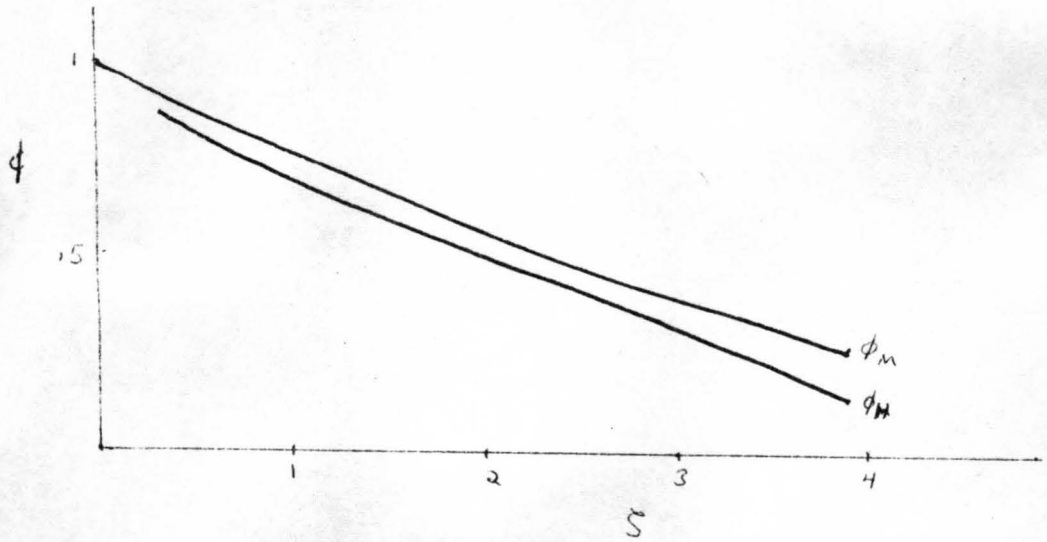

For very unstable regimes,

$$\phi_M = (1 - 16\zeta)^{-1/4} \tag{44}$$

$$\phi_V = \phi_H = (1 - 16\zeta)^{-1/2} \tag{45}$$

$$\alpha = \frac{\phi_M}{\phi_H} = \frac{K_H}{K_M} , \tag{46}$$

The observed dependence of α on ζ is shown in the figure below.

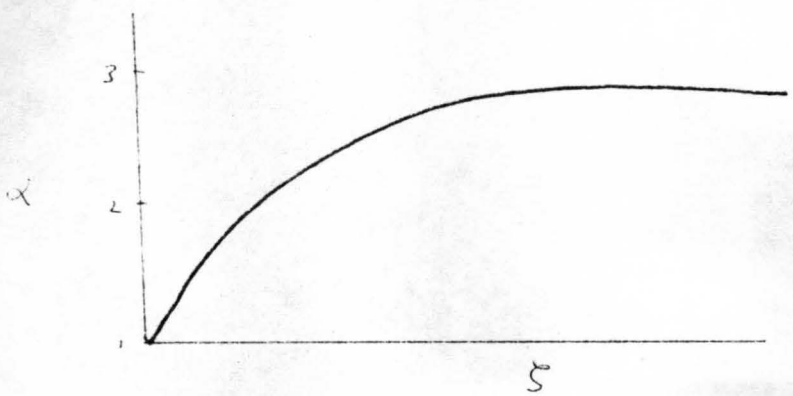

ELLISON - Small scale turbulence

Russian workers have tended to use the structure function to describe the energy in the small scales. For a scaler,

$$B(\tau) = \langle [\theta_{t-\tau} - \theta_t]^2 \rangle \tag{47}$$

The covariance function is

$$R(\tau) = \langle \theta_{t-\tau}\, \theta_t \rangle \tag{48}$$

so that

$$B(\tau) = 2(R_0 - R_\tau) . \tag{49}$$

The spectrum is defined by the Fourier transform of the variance function.

$$F(\omega) = \frac{2}{\pi} \int_0^\infty R(\tau) \cos \omega\tau \, d\tau . \tag{50}$$

The total energy of the scale field is then,

$$\langle \theta^2 \rangle = \int_0^\infty F(\omega)\, d\omega \tag{51}$$

If we extend our investigation to three dimensions,

$$R(\underset{\sim}{r}) = \langle \theta(\underset{\sim}{x} + \underset{\sim}{r})\, \theta(\underset{\sim}{x}) \rangle . \tag{52}$$

The spectrum is then given by

$$F(\underset{\sim}{k}) = \frac{8}{\pi^3} \int_0^\infty \int_0^\infty \int_0^\infty R(\underset{\sim}{r}) \cos(\underset{\sim}{k} \cdot \underset{\sim}{r}) \, dr_1 \, dr_2 \, dr_3 \, . \tag{53}$$

If the motion is isotropic, we only need be concerned with the magnitude of the vector $\underset{\sim}{k}$.

$$F(\underset{\sim}{k}) = f(|k|) = F(k) \, . \tag{54}$$

The total amount of energy between wave numbers of magnitude k and k + dk is given by

$$E(k) = 2\pi k^2 F(k) \, . \tag{55}$$

E(k) is called the three dimensional spectrum. What is usually measured, however, is $F_1(k)$ along the direction x_1. The one-dimensional spectrum, $F_1(k_1)$ is related to $F(\underset{\sim}{k})$ by

$$F_1(k_1) = \int\int F(k_1) \, dk_2 \, dk_3 \, . \tag{56}$$

If the flow is isotropic we have

$$F_1(k_1) = \int_{k_1}^\infty \frac{E(k)}{k} \, dk \, . \tag{57}$$

For a velocity, the problem becomes a bit more difficult.

$$E_u(k) = \frac{1}{2} k^3 \frac{d}{dk} \left(k^{-1} \frac{dF_{uu}}{dk} \right) \tag{58}$$

$$F_{vv}(k) = F_{ww}(k) = -\frac{1}{2} k^2 \frac{d}{dk}\left(k^{-1} F_{uu}\right) . \qquad (59)$$

If $F_{un} = Ak^{-\alpha}$, then $F_{ww} = A\, k^{-\alpha}\, \frac{(\alpha+1)}{2}$, and this leads to

$$E(k) = A k^{-\alpha} \frac{\alpha(\alpha+2)}{2} . \qquad (60)$$

Kolmogorov's second remark is that

$$E(k) = f(\varepsilon, \nu, k)$$

$$= \gamma\, \varepsilon^{2/3} k^{-5/3} j(k\lambda_s) , \qquad (61)$$

where $j(k\lambda_s)$ is a function of the wave number and the length scale formed by

$$\lambda_s = \nu^{3/4} \varepsilon^{-1/4} . \qquad (62)$$

If λ_s is sufficiently small, $j(k\lambda_s) = 1$.

$$\varepsilon = 2\nu \int_0^\infty k^2 E(k)\, dk . \qquad (63)$$

Many observations of the -5/3 law have been obtained. One difficulty with respect to the theory, however, is that the -5/3 regime extends too far towards the larger scales of motion. Eddies of size comparable to the height above the sea, and which are not isotropic, seem to lead to the -5/3 law.

In terms of the one-dimensional spectrum,

$$F_{uu} = \gamma_1 \varepsilon^{2/3} k^{-5/3} , \tag{64}$$

Observed values of γ_1 are as follows:

$\gamma_1 = .47 \pm .02$ in the sea

$\gamma_1 = .49 \pm .04$
$\gamma_1 = .44 \pm .02$
} in the atmosphere

Prior to about two years ago, the value of γ_1 agreed upon was $\gamma_1 = .48 \pm .01$.

Some observations have tended to underestimate the spectrum of the vertical velocity. Whereas F_{ww} should be equal to $4/3\ F_{uu}$, the observed coefficient in the atmosphere is often near unity (at least for those measurements near the ground). The observations of Myrup in an airplane, however, do give the value of 4/3 for the constant of proportionality.

The arguments that have been applied to the velocity field may also be applied to a scalar field. If ψ represents half the rate of scalar dissipation, we have,

$$F_s(k) = \gamma_s \psi \varepsilon^{-1/3} k^{-5/3} g_s(k\lambda_s, P_r) , \tag{65}$$

where p_r is the Prandtl number or Schmidt number, whichever the appropriate quantity may be. If diffusivity is much more important than the viscosity, the -5/3 power law will be cut off.

Values of γ_s for the one dimensional spectrum (γ_{1s}) are approximately .7 ± .1.

The spectrum equations may be used to estimate the dissipation (ε and ψ) from measurements at a single frequency. One can choose the frequency to suit one's particular instruments. If one could measure the dissipation using these ideas of Kolmogorow, one could then deduce the other terms in the energy equation as residuals (in order, for example, to estimate the shear stress).

Measurements obtained by Gibson during BOMEX resulted in values of $\gamma_1 \simeq .6$ and $\gamma_{1s} \simeq 2$. Observations in the laboratory, however, indicate that these coefficients are Reynolds number dependent.

Differences between the results of various workers suggest that quantities which are measured are perhaps not always consistent with the requirements of the Kolmogorow hypothesis. Small eddies must have a characteristic length which is less than the height above the boundary yet larger than the dissipation length.

If a ten centimeter eddy at a height of ten meters originated very near the boundary and was in fact comparable in size to the height above the boundary, that eddy would not satisfy the requirements of Kolmogorov's hypothesis when observed at a height of ten meters.

The use of the dissipation method to compute stress is particularly suspect over the sea (according to Frenzen) who found that under neutral conditions, production was not balanced by dissipation, thereby suggesting significant contributions from the divergence terms. The validity of the local dissipation concept, whereby the divergence terms are neglected, is even in doubt over flat in neutral conditions. If the local dissipation concept were valid, one could compute u_* for stability

conditions other than neutral. In fact, one could take measurements of velocity data at two heights in a constant flux layer, and obtain the heat flux.

ROLL - Air-sea transport processes

The turbulent velocity field will be defined by

$$\underset{\sim}{v} = (\bar{U} + u_1, u_2, u_3) .$$

The spectral density ϕ_{ij} is a function of the wave number $k = \frac{\partial \pi f}{\bar{u}}$ where f is the frequency.

$$\overline{u_i u_j} = \int_0^\infty \phi_{ij} \, df , \tag{66}$$

which is often written as

$$\int_{-\infty}^{\infty} f \, \phi_{ij} \, d(\ln f) . \tag{67}$$

We define $-\overline{u_1 u_3} = u_*^2$ and $u_* = k \, x_3 \frac{\partial \bar{u}}{\partial x_j}$. In terms of this notation,

$$\phi_{11} = \alpha_1 \, \varepsilon^{2/3} k^{-5/3} \tag{68}$$

In the case of isotropy, we have

$$\phi_{33} = \phi_{22} = \frac{4}{3} \phi_{11} . \tag{69}$$

Qualitative features of observations at sea are shown below.

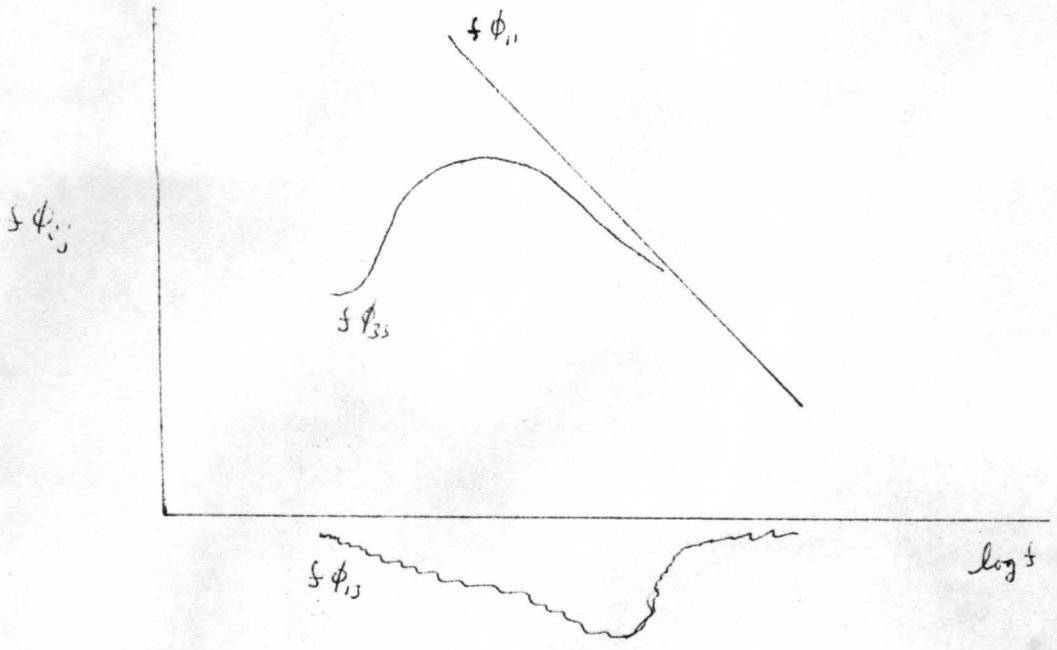

Vertical alignment of instruments is extremely important.

Observed drag coefficient (c_{10}) at ten meters x 10^3.

Smith (1967)	1.00 ± .27	Thrust anemometer	eddy correlation method
(Smiths data reanalyzed by Hasse)	1.03 ± .18		
Weiler and Burling (1967)	1.49 ± .41	Hot wire	
(Hasse reanalyzed above data)	1.31 ± .36		
Hasse (1968)	1.21 ± .24	Hot wire	
Smith (1969)	1.16 ± .42	Thrust anemometer	
Miyake (1970)	1.09 ± .18	Sonic anemometer	

Weiler (1967)	2.11 ± .53	Downwind spectral method (balance between production and dissipation)
Miyake (1967)	1.35	
Gibson	1.4 ± .02	

The downwind spectral method assumes isotropic turbulence, yet anisotropic conditions are often observed over the sea. There appears to be no appreciable dependence of c_{10} on wind speed, but there may be a dependence on stratification.

Transfer of sensible and latent heat.

$$\tau = \rho C_D \bar{U}^2 \tag{70}$$

where c_D and $\bar{U}$ are both evaluated at 10 meters.
The Jacobs formula for the heat flux is given by

$$H = - \rho C_p C_D \frac{K_H}{K_M} (U - U_s)(\theta - \theta_s) , \tag{71}$$

where the subscript s denotes the sea surface value. Likewise, the evaporation is given by

$$E = - C_D \frac{K_E}{K_H} (U - U_s)(q - q_s) . \tag{72}$$

It will be convenient to define some new coefficients

$$C_H = C_D \frac{K_H}{K_M} \tag{73}$$

$$C_E = C_D \frac{K_E}{K_M} \quad . \tag{74}$$

The value of c_D in the neutral case is denoted $(c_D)_N$.

Deardorf (1968) introduced the following form for a bulk Richardson number

$$Ri_v = \frac{g}{T_v} \frac{z}{(U-U_s)^2} \left[\theta - \theta_s + 0.61 \frac{C_E}{C_H} (q - q_s) \right] , \tag{75}$$

where T_V is the virtual temperature. Expressing that Richardson number in terms of the Monin-Obukhov length leads to

$$\frac{z}{L_v} = \frac{K \frac{C_H}{(C_D)_N}}{(C_D)_N^{1/2} \left(\frac{C_D}{(C_D)_N} \right)^{3/2}} \quad . \tag{76}$$

The vertical gradients of heat and moisture may be written as

$$\frac{\partial \theta}{\partial z} = \frac{\theta_*}{z} S_\theta \tag{77}$$

$$\frac{\partial q}{\partial z} = \frac{q_*}{z} S_q \quad . \tag{78}$$

A distinction must be made between stable and unstable conditions. In the unstable case, we assume

$$S_u = \left(1 - \gamma \frac{z}{L_v}\right)^{-1/4} \tag{79}$$

$$S_\theta = \left(1 - \gamma \frac{z}{L_v}\right)^{-1/2} \tag{80}$$

$$S_q = \left(1 - \gamma \frac{z}{L_v}\right)^{\mu} , \tag{81}$$

where $\mu = -1/4$ or $-1/2$. The value $\mu = -1/4$ corresponds to assuming that $K_E = K_M$, while the value $\mu = -1/2$ corresponds to assuming $K_E = K_H$. This is still an open question. Deardorf also assumed the value $\gamma = 16$, and that

$$\left.\begin{aligned} \theta - \theta_s &= 0 \\ q - q_s &= 0 \\ u - u_s &> 0 \end{aligned}\right\} \quad z = z_0$$

In the stable case,

$$S_u = 1 + \alpha_u \frac{z}{L_v} \tag{82}$$

$$S_\theta = 1 + \alpha_\theta \frac{z}{L_v} \tag{83}$$

$$S_q = 1 + \alpha_q \frac{z}{L_v} \tag{84}$$

Deardorf used the values $\alpha_u = 7$, $\alpha_\theta = 11$, and $\alpha_q = 20$ to obtain results that are indicated below in a qualitative manner.

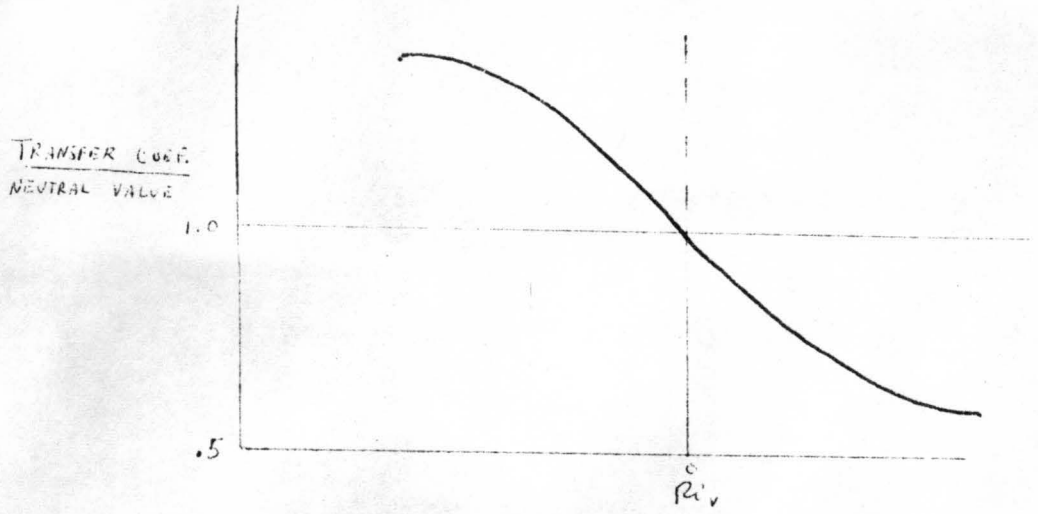

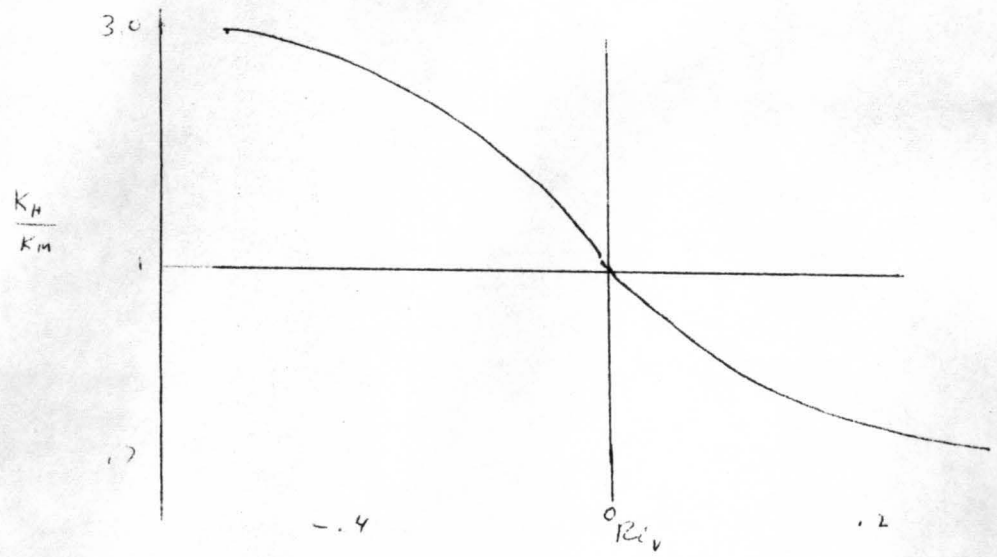

Processes at the sea surface seem not to be very well understood at the present time. There are indications, for example, that the actual temperature of the sea surface may be cooler than present methods indicate. The temperature gradient in the lowest 10 cm of the atmosphere has been found to exceed the gradient in the uppermost 10 cm of the ocean by a factor of 20. The actual sea surface may have a "cool skin" which is approximately half a degree cooler than the values indicated by present methods.

A study by McAllister and McLeish (1969) gives the following picture of the fraction of heat transported by conduction, radiation, and turbulence as a function of height.

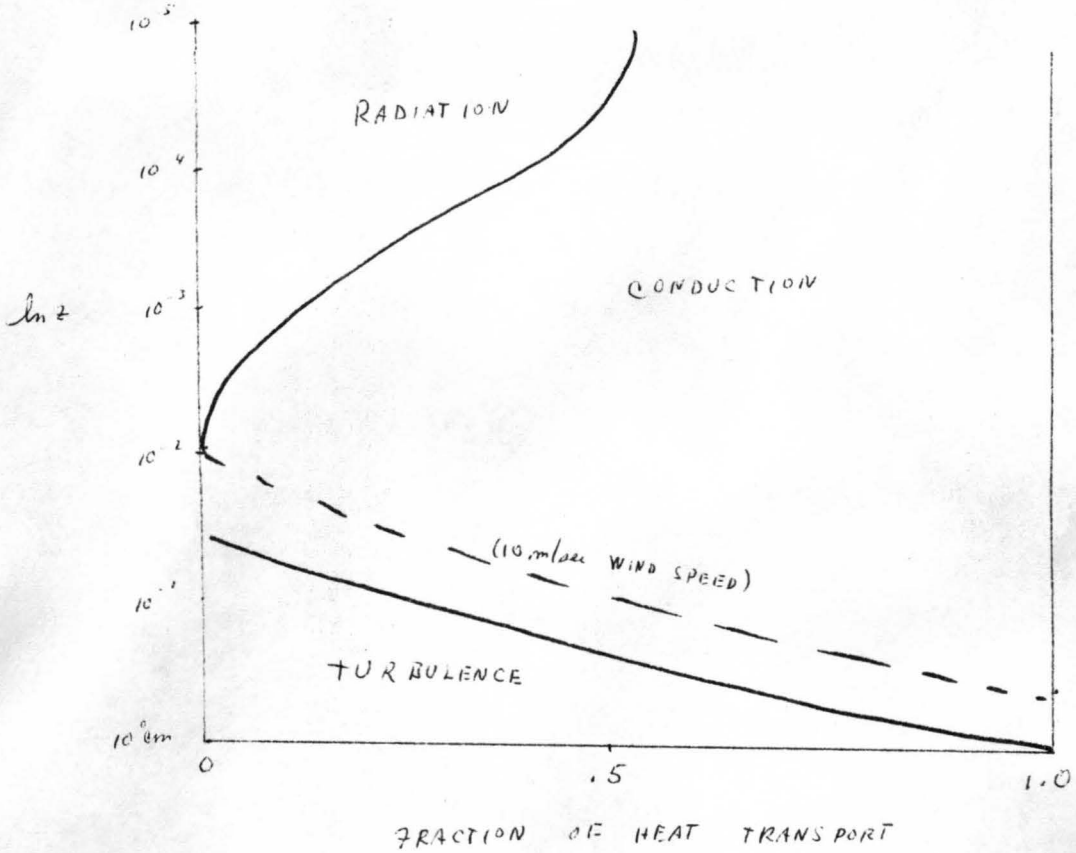

Surface tension associated with a monomolecular layer acts as a strong barier to evaporation.

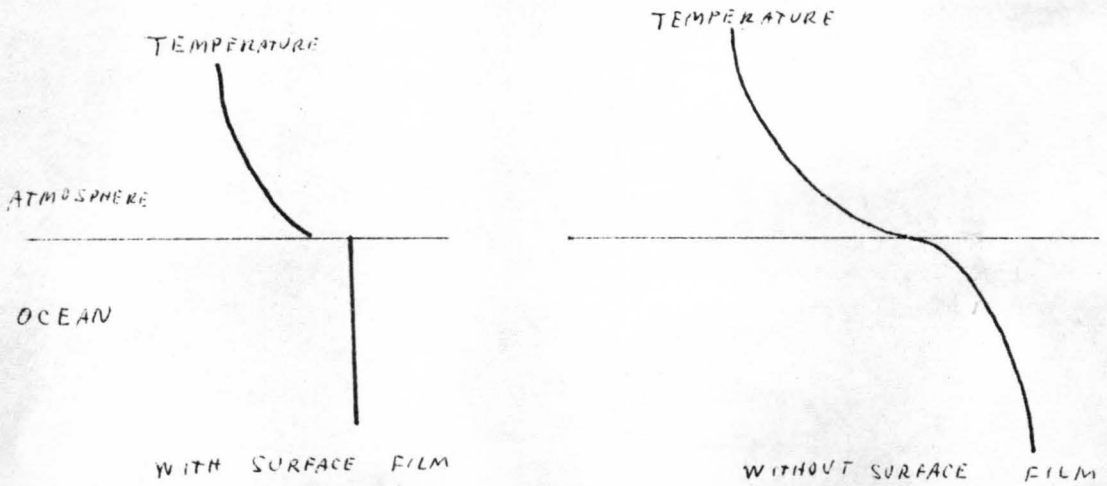

Momentum and heat transfer at the sea surface may also be affected by sea spray. Some studies in the laboratory indicate a significant increase in sea spray when the wind speed increased to about 12 to 13 m/sec. Field measurements of the number of spray droplets as a function of wind speed lead to the following picture.

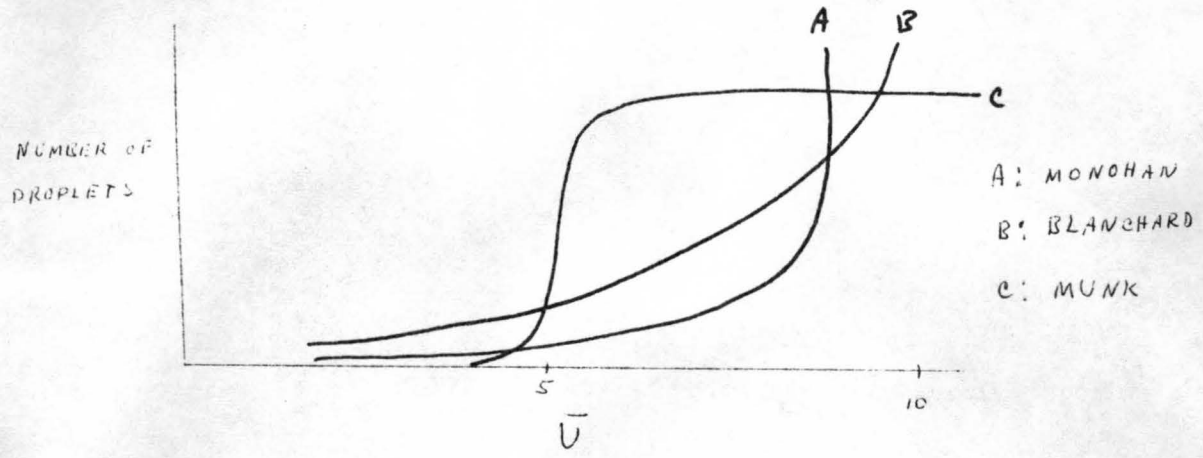

The overall conclusion that can be reached is that we have reached a relatively advanced state of knowledge regarding the small scale processes at low wind speeds, but that due to the hostile nature of the ocean, advances in our knowledge at the higher speeds will probably be made by indirect methods of measurement.

The critical wind speed at which the number of spray droplets suddenly increases will be higher over fresh water than over the ocean.

"Humps" have been observed in the humidity spectrum over sea (Gibson) and in the temperature spectrum over land (Busch). Because of the fact that their measured values of production exceeded dissipation. Busch suggests that those humps in the -5/3 law are associated with an energy concentration in a particular frequency band which is being exported as a flux divergence.

DORRESTEIN - Characteristics of surface waves (see abstract)

The concepts of deep and shallow water waves may be examined in terms of the equation

$$c^2 = \frac{g}{k} \tanh kd \tag{85}$$

$$c^2 = \frac{g}{k} \qquad \text{(DEEP WATER WAVES)} \tag{86}$$

$$c^2 = gd \qquad \text{(SHALLOW WATER WAVES)}, \tag{87}$$

Energy of the waves propagates at the group velocity, c_g. If $c^2 = \sigma/k$, $c_g = \partial\sigma/\partial k$.

The maximum angle at the crest of two-dimensional, irrotational waves is 120^o. The maximum angle for two dimensional standing waves is 90^o, however.

Let us consider a wave distribution such as that indicated below.

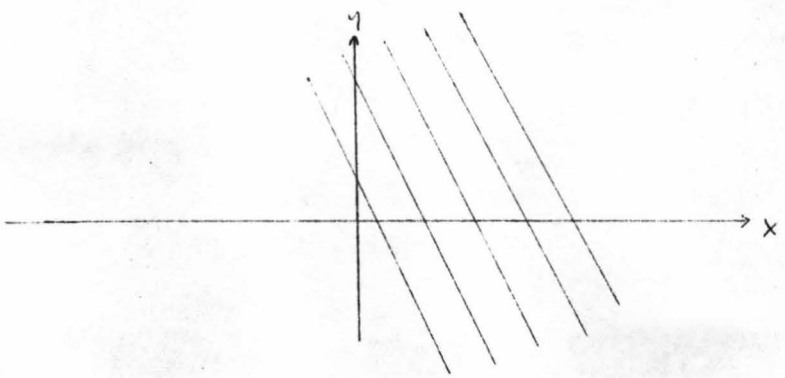

This wave may then be replotted in wave number space.

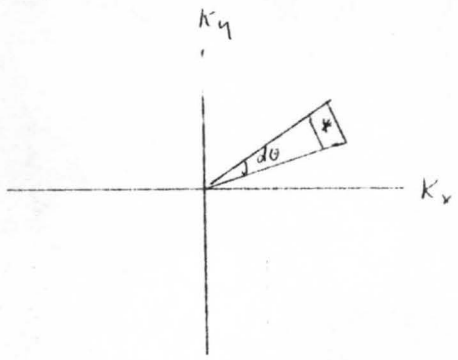

the height variance is given by

$$\overline{\zeta^2} = \iint dk_x\, dk_y\, \psi(k_x, k_y)$$

$$= \iint k\, dk\, d\theta\, \psi(k\cos\theta, k\sin\theta)\,, \tag{88}$$

where k is the magnitude of the vector with components k_x and k_y. In deep water, $k = \sigma^2/g$, or $dk = 2\sigma d\sigma/g$, which leads to the following expression for deep water waves.

ONE DIMENSIONAL FREQUENCY SPECTRUM

$$\overline{\zeta^2} = \int_0^\infty d\sigma \left[\int_0^{2\pi} d\theta \left\{ \frac{2\sigma^3}{g^2}\, \psi\left(\frac{\sigma^2}{g}, \theta\right) \right\} \right] \tag{89}$$

DIRECTIONAL FREQUENCY SPECTRUM

The spectrum of a fully developed sea is shown below.

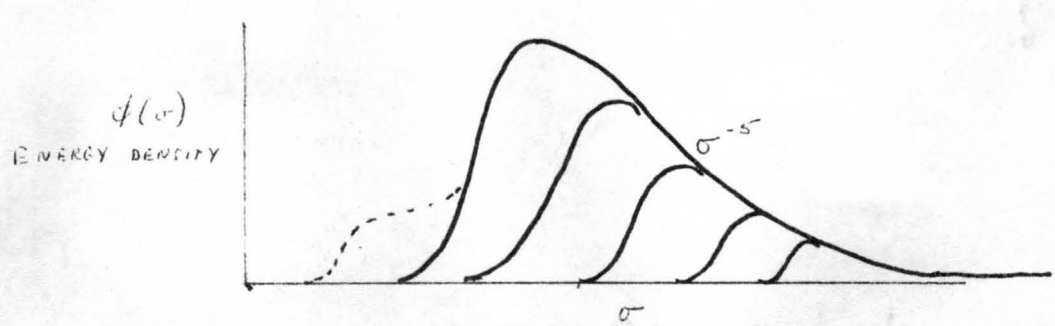

In the equilibrium range, $\phi(\sigma) = \beta\, g^2 \sigma^{-5}$. The constant, β, has been found by various investigators to lie between about 0.8×10^{-2} and 1.5×10^{-2}. Phillips, however, says that β is not a constant but varies with wave height. Hide and Plate report a value of $\beta = 2.10 \times 10^{-2}$ in their wind-water tunnel.

Fetch limited waves tend to overshoot the equilibrium spectrum in the manner shown below.

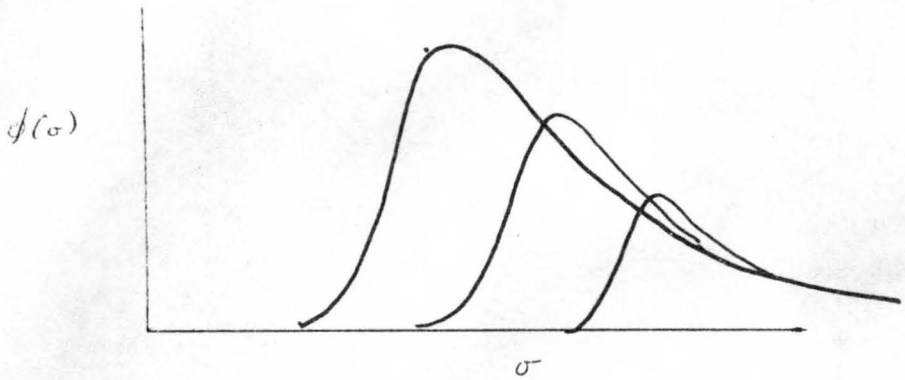

RODGERS - Radiation budget

The total flux of energy impinging on the earth from the sun is $1400\ \pi R^2$ watts/m^2, which results in an equilibrium radiation temperature of approximately 250° absolute. If we consider the total budget for the earth as a whole, we obtain the following amounts (based on an incoming value of 100 units).

Incoming = 100		Outgoing	
Reflected by cloud	27	Emitted by atmosphere to space	55
" " air	7	" " " " surface	96
Absorbed by cloud	12	" " surface to atmosphere	108
" by air	8	" " " to space	8
Absorbed by surface (direct)	27		

Absorbed by surface (diffuse)	16		
reflected by surface	5		
surface gain	43	surface loss	20

The difference between surface loss and gain is accounted for by turbulent transport (4 units) and by the transport of latent heat (19 units). Radiation in the atmosphere interacts primarily with H_2O and CO_2 .

RODGERS - Radiative equilibrium.

The temperature at the equatorial tropopause is lower than at the polar tropopause. A net radiation loss at the poles and net radiation excess at the equator is compensated for by a net poleward transport of heat.

Radiation effects may be incorporated into the heat equation by introducing an artificial conductivity term.

$$K_r = \frac{16 \pi T^3 \sigma}{k} , \qquad (90)$$

where k is the absorption coefficient, and the T^4 relationship has been invoked. If one inserts typical values for the various parameters into the equation, one finds that the radiation conductivity is larger than the molecular conductivity. Radiation effects should be taken into account for decay times of the order of 100 seconds. Radiation reduces the buoyancy of a parcel of air and enhances the production of turbulent eddies. In the boundary layer, the critical Richardson number (for the development of turbulence) for small eddies is increased by a factor of approximately 2.5. The critical Richardson number for the troposphere

as a whole is increased by a factor of approximately 2.0. The Richardson number at which turbulence will decay will not, however, necessarily be increased by this factor. More experiments need to be carried out to further investigate the effects of radiation on turbulence.

DORRESTEIN - Momentum and energy transport in surface waves.

The Stokes drift for a fully developed sea has been computed by Bye (1967).

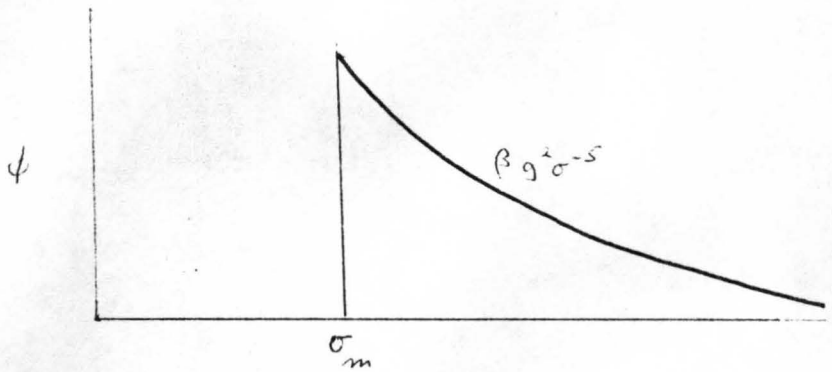

The surface drift in terms of the cut off frequency, σ_m is given by

$$U_s = \frac{3\sigma}{\sigma_m} \tag{91}$$

where σ_m is in seconds, and U_s is in cm/sec. For a wind speed of 10 m/sec, $\sigma_m = \frac{2\pi}{7}$, which leads to a value of 35 cm/sec for the surface Stokes drift. Wright (1970) showed that the Stokes drift would be smaller in a developing sea. Kenyon (1970) obtained the following relation between the Stokes transport and the Ekman transport

$$\frac{T_s}{T_E} = .016\, U_{10} \tag{92}$$

where U_{10} is the velocity at 10 meters.

Let us now consider the following two-dimensional flow.

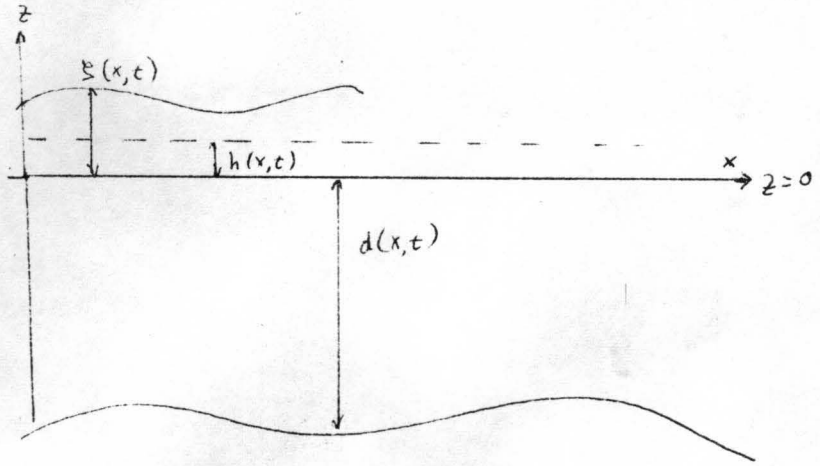

The vertically integrated equations are

$$\frac{\partial}{\partial t}\int_{-d}^{\zeta}\rho u\,dz + \frac{\partial}{\partial x}\int_{-d}^{\zeta}\rho u^2\,dz = -\frac{\partial}{\partial x}\int_{-d}^{\zeta}p\,dz + P_d\frac{\partial d}{\partial x}, \tag{93}$$

where P_d is the bottom pressure and $\frac{\partial d}{\partial x}$ the slope of the bottom, We now let $P = \rho g(\zeta - z) + P'$, and average over a number of wave periods. Also, $\zeta' = \zeta - h$.

$$\frac{\partial}{\partial t}\int_{-d}^{\zeta}\rho u\,dz + \frac{\partial}{\partial x}\left[\int_{-d}^{\zeta}(\rho u^2 + p')\,dz + \tfrac{1}{2}\rho g\overline{\zeta'^2}\right] = -\rho g(d+h)\frac{\partial h}{\partial x}, \tag{94}$$

where the second term on the left represents the so-called radiation stress or a vertically integrated pressure, and where $\frac{\partial h}{\partial x}$ represents the mean slope of the sea surface. If a mean current also exists, that is, if $u = U + u_{waves}$, we must add to the left side of the previous equation

$$\frac{\partial}{\partial t}\left[\rho U(d+h)\right] + \frac{\partial}{\partial x}\left[\rho U^2(d+h) + \tfrac{1}{2} U M_{waves}\right], \tag{95}$$

where $M_{waves} = \int_{-d}^{\zeta} \rho u_{waves} dz$. (96)

Let us now make the approximation $\overline{p'} = -\rho \overline{w^2}$, where w is the vertical velocity. For a periodic wave in deep water, the first order term $\overline{u^2 - w^2} = 0$, so

$$S = \tfrac{1}{2} E \tag{97}$$

where E is the energy density. For a periodic wave in shallow water we neglect w with respect to u.

$$S = \tfrac{3}{2} E = \left(\frac{2 c_g}{c} - \frac{1}{2} \right) \tag{98}$$

where c_g is the group velocity of a single wave.

CHARNOCK - Characteristic diagram

The best observed quantity in both the atmosphere and ocean is the temperature. The next best observed quantity is the humidity in the atmosphere and the salinity in the ocean. The velocity comes in a poor third in both the atmosphere and ocean.

A characteristic diagram has the property that the two axes represent "conservative" quantities. Conservative diagrams for the atmosphere and ocean are of the type indicated below.

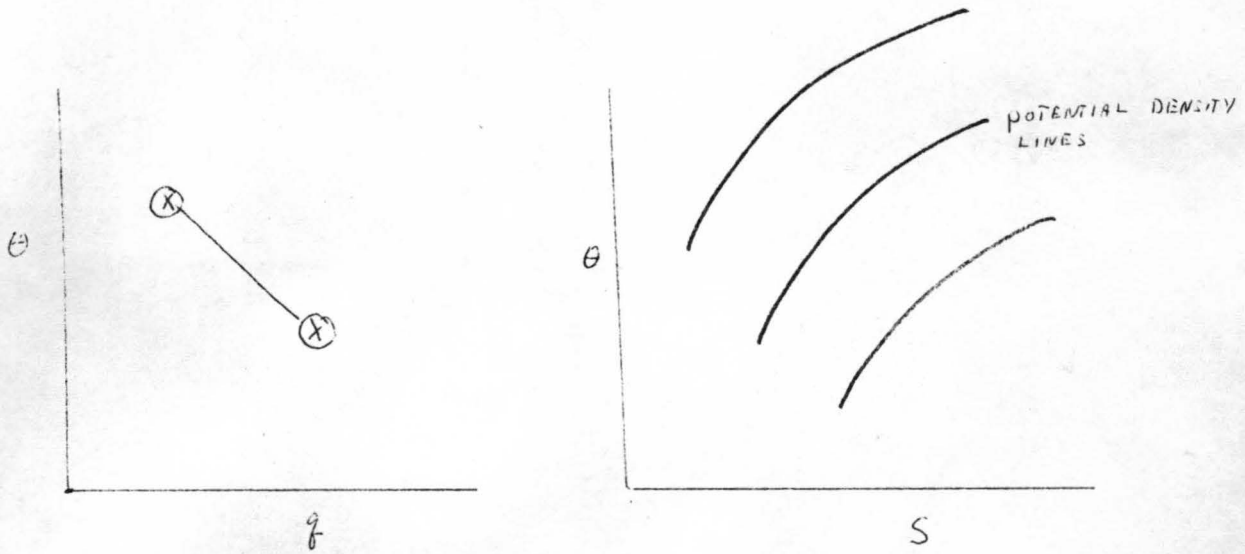

θ represents potential temperature, q represents specific humidity, and s represents salinity.

Molecular processes are quite important in the ocean but apparently not so important, in the atmsphere. Salt diffuses much more slowly, for example, than heat. Whereas mixtures in the atmospheric characteristic diagram between two blobs of air tend to occur along straight lines, mixtures in the ocean between two water masses tend to follow curved paths such as those indicated in the examples considered below.

CASE 1. $\overline{T}_1 > \overline{T}_2$

$S_1 < S_2$

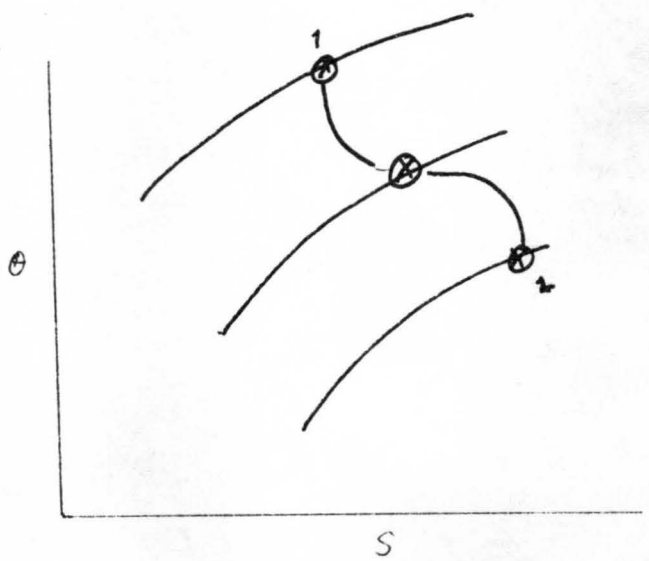

CASE 2. $\bar{T}_1 > \bar{T}_2$

$S_1 > S_2$

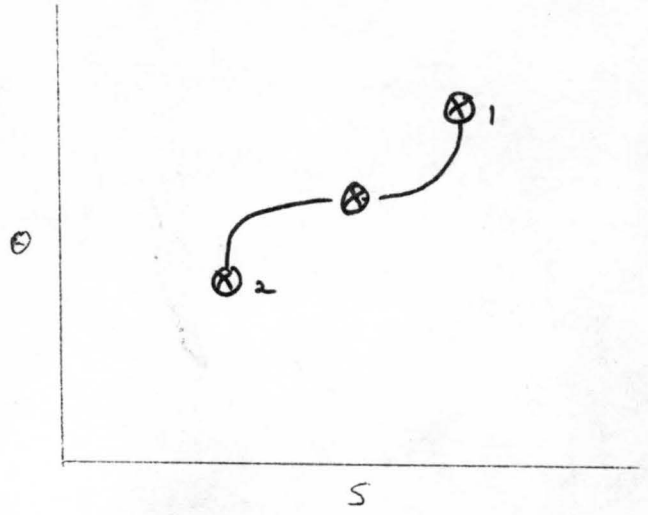

Case 2 corresponds to conditions associated with salt fingers.

CASE 3. $\bar{T}_1 < \bar{T}_2$

$S_1 < S_2$

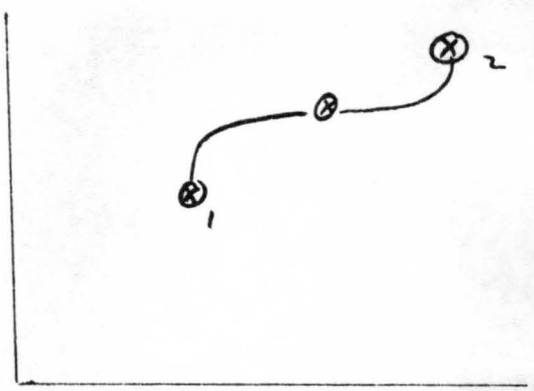

Case 3 corresponds to conditions associated with convection and layering.

The bottom of the ocean has a constant potential temperature rather than a constant temperature. This observation implies transfer processes are carried out primarily by the motion of blobs of fluid rather than by molecular processes.

SIMPSON - Oceanic energy balance

The energy budget for an ocean column of unit area may be expressed as

$$R = Q_s + Q_e + S + Q_{vo} \tag{99}$$

where R represents the net incoming radiation, Q_s the flux of sensible heat to the atmosphere, Q_e the flux of latent heat to the atmosphere, s the heat storage of the ocean, and Q_{vo} the flux divergence. The energy supplied by the sea to the atmosphere is then

$$Q_s + Q_e = R - S - Q_{vo} \quad , \tag{100}$$

where Q_e = LE. S is assumed to be zero when one averages over a period of one year. However, seasonal variations in S may amount to 1/3 of Q_e. The term Q_{vo} is usually ignored or computed as a residual due to a lack of observational data.

The Jacobs transfer formulas which are often used to compute the fluxes of sensible and latent heat are given by

$$Q_s = B_s C_p (T_o - T_a) U_a \tag{101}$$

$$Q_e = B_e L (q_o - q_a) U_a \quad , \tag{102}$$

where the subscript o refers to the ocean surface, and the subscript a refers to the anemometer level of about 6 meters where the wind speed is usually measured. These equations are appropriate for near neutral conditions in which there exists a logarithmic velocity profile. Under unstable conditions, the transfer formulas will result in a 40% error

when the Richardson number approaches -.2. A 40% error may be expected under stable conditions for Richardson numbers of order .02.

The Bowen ratio is expressed by

$$r = \frac{Q_s}{Q_a} = \frac{c_p}{L} \frac{(T_o - T_a)}{(q_o - q_a)} \quad , \tag{103}$$

where the transfer coefficients are assumed to be equal.

Since the transfer formulas are proportional to the wind speed, most of the transfer occurs when the wind speed is high. High wind speeds at the anemometer level will then correspond to small Richardson numbers. The transfer formulas are therefore particularly valid where the bulk of the transfer is actually occurring.

The net incoming radiation at the sea surface is determined by the equation

$$R = (Q + q)(1 - \alpha) - Q_b \quad , \tag{104}$$

where Q is the direct short wave radiation, q is the diffuse short wave radiation, α is the albedo of the sea surface and Q_b the effective outgoing radiation.

The critical variable in the determination of R is the atmsopheric cloudiness. Empirical correction formulas for the cloudless parameters have been determined as a function of latitude and season

$$Q + q = (Q + q)_o (1 - a n^b) \tag{105}$$

$$Q_b = (Q_b)_0 (1 - c n^d) \quad , \tag{106}$$

where n represents the mean fractional cloudiness. Since the constants b and a have been found to be nearly equal to unity, we may combine the equations to obtain the following result,

$$R \approx A - Bn \quad . \tag{107}$$

Let us now consider a particular example at 20°N in February. If we neglect the storage and flux divergence terms, we have

$$Q_e = \frac{R}{1+r} \quad . \tag{108}$$

The resulting effect of cloudiness on Q_e is then indicated below.

n	Q_e
0	11.1 Kg cal/cm² month
40%	7.5
100%	3.3

The net incoming radiation will depend on the type and thickness of the cloud cover. The fact that the simple formulas give reasonable results must be due to the reproducibility of the cloud cover at a given latitude at a given month. The empirical constants take into account variations in types of cloud cover. Improvements in the evaluation of

the effects of cloudiness on the net radiation should be forthcoming with the use of satellite data.

Budget studies in the Northern hemisphere have shown that the oceanic flux divergence is positive south of 30^{o} latitude and negative to the north of that latitude, with values approaching 1/3 of Q_e. The oceanic flux divergence is therefore not negligible in budget studies.

Evaporation of sea water and the resulting transfer of latent heat is the primary mechanism for the transfer of the net radiative energy from ocean to atmosphere. Typically, the transfer of sensible heat is only one or two tenths the transfer of latent heat.

SIMPSON - Air sea interaction on the synoptic scale

Let us consider a column of unit area extending from the bottom of the ocean to the top of the atmosphere. The radiation balance for the entire column may be expressed as

$$R_s = L(E-P) + Q_{vo} + Q_{va} \tag{109}$$

$$L(E-P) = Q_{vw} \quad , \tag{110}$$

where the storage terms have been neglected since we are considering an annual average. The term (E-P) represents the difference between evaporation and precipitation, and hence may be interpreted as a flux divergence of water vapor transport in the atmosphere. The term Q_{va} is very nearly the flux divergence of sensible heat plus potential energy (realized energy). Q_{va} may be computed as a residual and then compared with aerological data.

The trade wind regions act as accumulators of latent heat. This latent heat is transported to the equatorial convergence zone where cumuloriumlus clouds convert the latent heat into sensible heat and lift it to great heights.

ELLISON - Energy spectra

Turbulent signals are in general highly intermittent. A consequence of this intermittency is that

$$\langle \varepsilon \rangle^{2/3} \neq \langle \varepsilon^{2/3} \rangle \quad , \tag{111}$$

and that one must be careful in evaluating the terms in -5/3 law.

If one has a cascade process of turbulent energy, these cascade processes will produce fluctuations in ε . After a sufficiently large number of steps in the cascade process, the probability distribution of log ε must become normal. This result should also be true of the components of ε and the measurements of $(\frac{\partial u}{\partial x})^2$ seem to verify this normal distribution.

Let us write $\varepsilon = \varepsilon_o e^n$. The probability distribution is then

$$p(\eta) = (2\pi)^{1/2} \sigma^{-1} e^{-\eta^2/\sigma^2} \quad , \tag{112}$$

where σ is the variance. The mean value of $\langle \varepsilon^\alpha \rangle$ is given by

$$\langle \varepsilon^\alpha \rangle = \varepsilon_o^\alpha e^{\frac{1}{2}\sigma^2\alpha^2} \quad , \tag{113}$$

The Kurtosis of $\frac{\partial u}{\partial x}$, given by $\frac{\langle (\frac{\partial u}{\partial x})^4 \rangle}{\langle \frac{\partial u}{\partial x}^2 \rangle}$, should be 3 if $\frac{\partial u}{\partial x}$ were normally distributed. The probability distribution considered above would result in very large values of the Kurtosis, depending of course on the value of the variance. Measured values typically are of order 15.

For a three dimensional spectrum

$$E_\eta(k) = a_{12} k^{-1} . \tag{114}$$

The variance of η is given by

$$\sigma^2 = \int_{L^{-1}}^{\lambda_s^{-1}} E_\eta(k)\, dk , \tag{115}$$

where L is the scale of the large scale motions (the scale at which the energy is fed in), and λ_s is related to the Kolmogorov length. If one has a filter, however, one only integrates to some cutoff wave number k'.

If we have a large scale Reynolds number

$$\frac{L}{\lambda_s} \propto Re^{3/4} , \tag{116}$$

where $Re = LU/\nu$, one can then obtain

$$\sigma^2 = a_{12} \ln\left(\frac{L}{\lambda_s}\right) = \frac{3}{4} a_{12} \ln(Re) . \tag{117}$$

The variance therefore increases with Reynolds number. If we are interested in some particular scale, K such that $K \lambda_s << 1$, the viscosity is not important.

Let us consider the one-dimensional function

$$F_\xi(k) = \frac{1}{2\pi} \int \langle \xi(x)\,\xi(x+r) \rangle \cos(kr)\, dr$$

$$= \frac{\langle \xi^3 \rangle}{2\pi} e^{-\sigma^2} \int_0^\infty \langle e^{\eta(x)+\eta(x+r)} \rangle \cos kr\, dr . \qquad (118)$$

One can obtain,

$$F_\xi(k) = \frac{k^{-1}}{2\pi} (-a_{12})!\, \sin\left(\frac{\pi a_{12}}{2}\right) (4.71\, kL)^{a_{12}} . \qquad (119)$$

The coefficient a_{12} has been found to be very nearly minus one half. For $\sigma^2 = a_{12} \ln(LK)$,

$$E(k) = \gamma \langle \varepsilon \rangle^{2/3} k^{-5/3} (Lk)^{-a_{12}/9} \qquad (120)$$

The resulting change in the power of K, which is $-a_{12}/9 = 1/18$, is not measurable.

TURNER - Turbulent entrainment

Similarity approach for convection from small sources may be used to investigate the following three situations.

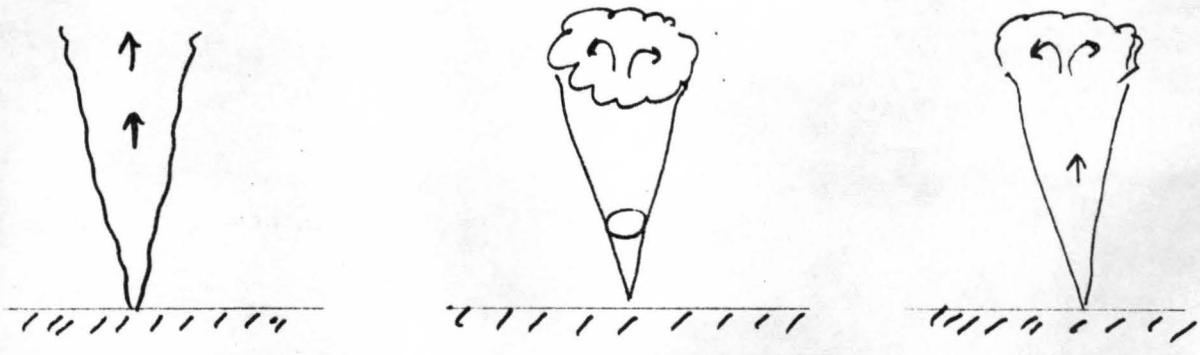

We shall use the Boussinesq approximation in which density differences are neglected except when they occur in conjunction with gravity.

The first case to be considered is that of a plume located in an environment of constant potential temperature.

The instantaneous boundary between plume and environment is quite sharp, but the time average at point near the mean location of the plume edge would be more nearly Gaussian.

From similarity considerations it can be shown that the properties are determined by the height, and the buoyancy flux.

$$\rho_0 F = g(\rho - \rho_0) V_F \tag{121}$$

where V_F is the volume flux from the source.

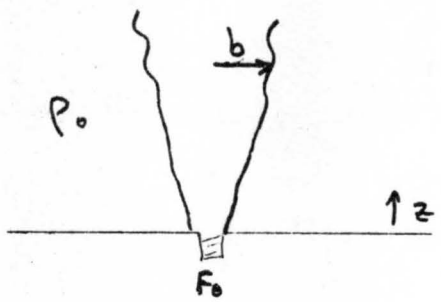

The radius (a characteristic dimension) of the plume, the vertical velocity, and the $g\frac{(\rho-\rho_0)}{\rho_0}$, will be written as

$$b \propto F^l z^m \tag{122}$$

$$w \propto F^c z^d f_1\left(\frac{r}{b}\right) \tag{123}$$

$$\Delta = \frac{g(\rho-\rho_0)}{\rho_0} \propto F^j z^k f_2\left(\frac{r}{b}\right) . \tag{124}$$

From dimensional considerations, we find that $c = 1/3$, $d = -1/3$, $j = 2/3$, $k = -5/3$, which leads to

$$b \propto z \tag{125}$$

$$w \propto F^{1/3} z^{-1/3} f_1\left(\frac{r}{b}\right) \tag{126}$$

$$\Delta \propto F^{2/3} z^{-5/3} f_2\left(\frac{r}{b}\right) . \tag{127}$$

The proportionality constants which were determined experimentally, are

$$w = 4.7\, F^{1/3} z^{-1/3} \exp\left(-96\, r^2/z^2\right) \tag{128}$$

$$\Delta = 11.0\, F^{2/3} z^{-5/3} \exp\left(-71\, r^2/z^2\right) . \tag{129}$$

Since these solutions blow up as z tends to zero, they should only be expected to be valid some distance above the source.

The solutions show that the mass flux is not conserved but is proportional to $z^{5/3}$. Fluid is entrained into the fluid at a rate proportional $z^{-1/3}$ times the surface area, which is proportional to the mean vertical velocity. That is, the mean inflow velocity is proportional to the mean upward velocity. If one assumes that relation, one has

$$\text{CONSERVATION OF MASS:}\quad \frac{d}{dz}\left(b^2 w\right) = 2\alpha b w \tag{130}$$

CONSERVATION OF MOMENTUM: $$\frac{d(b^2 w^2)}{dz} = b^2 w \tag{131}$$

CONSERVATION OF BUOYANCY: $$\frac{d(b^2 wA)}{dz} = b^2 w \frac{g}{\rho} \frac{\partial \rho_a}{\partial z}, \tag{132}$$

where the last equation has been extended to the case of a non-uniform environment. In neutral conditions, $\alpha \approx .08$.

In the case of a forced plume, we must specify the fluxes of buoyancy and momentum. If M represents the momentum flux, one can obtain,

$$z = \alpha^{-1/2} M^{3/4} F_o^{-1/2} z_1 \tag{133}$$

$$b = \alpha^{1/2} M^{3/4} F_o^{-1/2} b_1 \tag{134}$$

$$w = \alpha^{-1/2} M^{-1/4} F_o^{1/2} w_1, \tag{135}$$

where z_1, b_1, and w_1 are non-dimensional functions of the height variables.

Thermals may be analyzed in a similar manner, resulting in the relations

$$b = \alpha z \tag{136}$$

$$w \propto F_*^{1/2} z^{-1} \tag{137}$$

$$A \propto F_* z^{-3}, \tag{138}$$

where $F_* = \frac{g\Delta\rho}{\rho} V$, the total buoyancy, which remains constant.

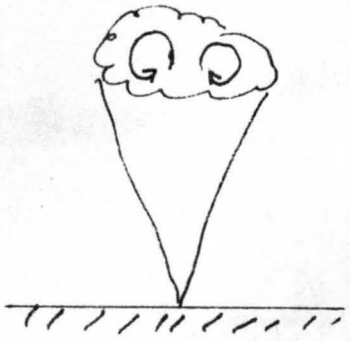

The continuity equation for the thermal may be written as

$$\frac{d}{dt}\left(\frac{4}{3}\pi b^3\right) = 4\pi\alpha b^2 w \,, \tag{139}$$

which implies that

$$\frac{1}{V}\frac{dV}{dz} = \frac{3\alpha}{b} \,, \tag{140}$$

where V is the volume. Also,

$$\frac{db}{dz} = \alpha \,, \tag{141}$$

independent of the momentum equations. (The momentum equation is necessary in order to obtain $\frac{db}{dz}$ for the plume).

The thermal may be considered as a special case of a buoyant vortex ring, whose angle of spread is determined by the ratio the buoyancy flux to the square of the circulation.

The starting plume is found to spread more slowly than a thermal.

The ideas previously presented may be extended to unstable and stable environments. In the unstable case, similarity solutions can be obtained for particular environments. For power law environments, i.e.,

$$\frac{g}{\rho}\frac{d\rho}{dz} = C z^{p} \tag{142}$$

one finds

$$\Delta = c\left(4 + \frac{3p}{2}\right)^{-1} z^{(1+p)} \tag{143}$$

If for example p = -4/3, which corresponds to a power law appropriate to free convection, one obtains,

$$w \propto z^{1/3} \tag{144}$$

$$\Delta \propto z^{-1/3} . \tag{145}$$

Power laws are not appropriate for a stable environment because a thermal would then come to rest at some finite height.

Let us consider a plume in a constant stable density gradient,

$$-\frac{g}{\rho_0}\frac{d\rho_0}{dz} = G . \tag{146}$$

One then obtains,

$$z = \alpha^{-1/2} F_0^{1/4} G^{-3/8} z_1 . \tag{147}$$

Experimental determinations of the maximum height of plume rise lead to a value of $5.0\ F_0^{1/4}\ G^{-3.8}$. A surprising result in the case of a forced plume (for substantial rates of injection) is that the final heights are reduced due to an increased mixing with the environment. The fluid near the source acts more like a jet.

For buoyant vortex rings, the maximum height is proportional to $F_*^{-1/2} K_o^{3/2} G^{-1/4}$, where K_o represents the circulation. The maximum height can therefore be increased by increasing the the circulation, which corresponds to increasing the rate of injection.

SIMPSON - Cloud dynamics and modification experiments

Some of the most useful models of cumulus clouds have been based on the laboratory experiments of Turner, et at. The plume, starting plume, and thermal all have some degree of similarity to some stage of a cumulus cloud. The main difference between laboratory models and cumulus cloud is the existence of a phase change in real clouds.

Entrainment rates for small non-precipitating cumulus clouds are of the order $\frac{1}{M} \frac{dM}{dz}$ 10^{-5} cm^{-1}. An entrainment rate of 10^{-5} cm^{-1} may be interpreted as a doubling of the cloud volume due to mixing in of environmental air during a rise of one kilometer. Entrainment into a cumulus cloud is very much affected by the existence of a mean wind shear in the environment. Entrainment is found to occur on the up-shear side, while detrainment, or the shedding of moist air, occurs on the downshear side. Entrainment is apparently inversely proportional to cloud diameter.

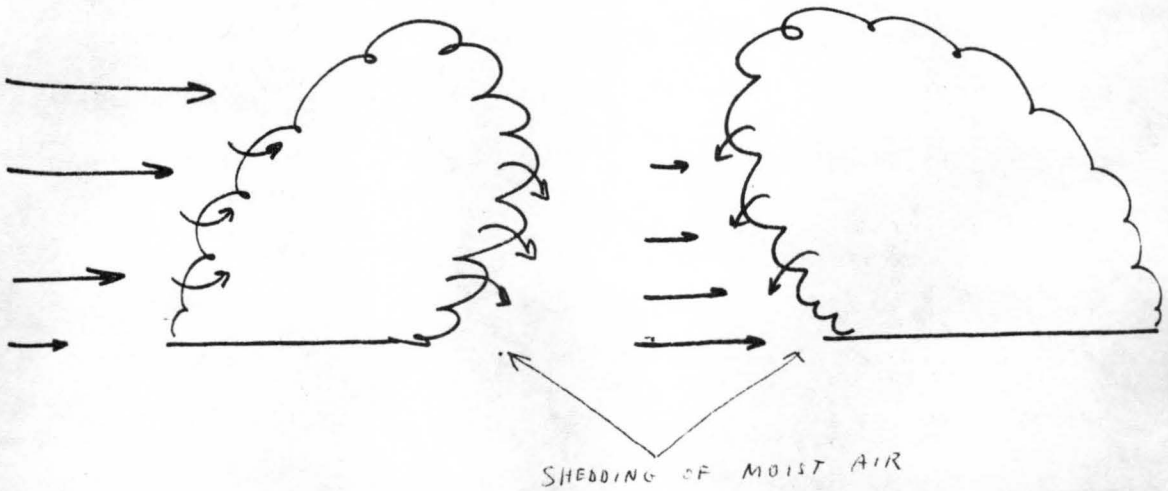

The temperature of a typical cumulus cloud exceeds that of its environment by approximately one half to one degree centigrade. If 3 grams per kilogram of water at 20,000 feet were to freeze, the resulting increase in temperature of one degree centigrade would double the buoyancy of the cloud. Dynamic seeding experiments have been carried out in order to ascertain whether or not the injection into a cloud of a material such as silver iodide would act as a triggering mechanism, leading to a rapid growth of the cloud. Results of a number of seeding experiments have led to a very good correlation between seeding and the subsequent growth of cumulus clouds.

The increased vertical growth resulting from the seeding of a cloud is what is called the seedability of that cloud. A cumulus cloud model has been developed to predict this seedability. If Δz_s represents the difference between the predicted top height of the cloud and the unseeded top height, and Δz_o represents the actual observed difference between the top height of the cloud and the unseeded top height, one may use these height differences to indicate the success of a seeding program.

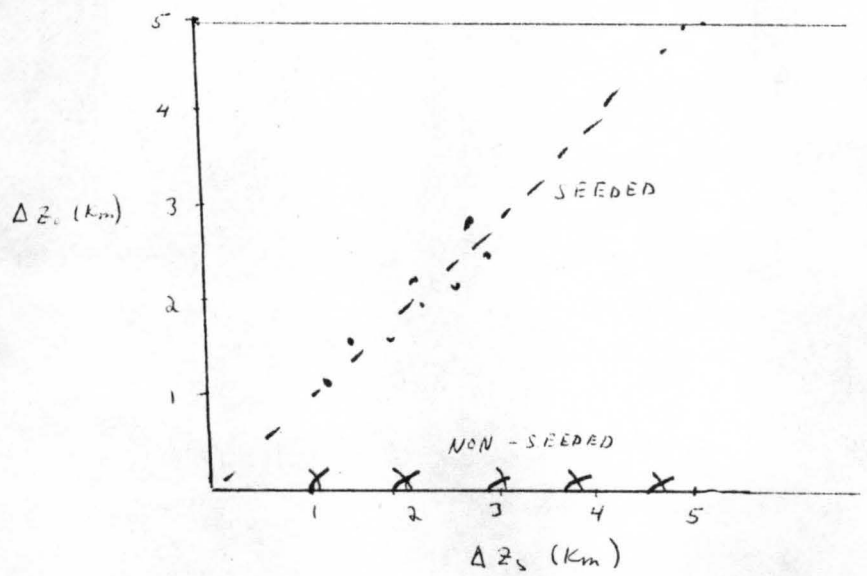

The results of a 1965 randomized seeding experiment in the Caribbean are shown in the graph above. The seeded and unseeded clouds separate with a statistical significance of better than one percent.

Three different growth regimes have been observed following the seeding of cumulus clouds. The first regime consists of an explosive growth in which precipitation is greatly enhanced and may in fact be doubled. The second regime may be called the "cut off tower regime," in which the top separates and the main cloud dies. The third regime has no growth whatsoever.

The equation for the rate of rise of the cap of a cloud is equally valid for plumes, starting plumes, and thermals, the only difference being that different experimental constants must be used corresponding to the appropriate type of convective element. A comparison of the predictions with field results indicates that the most consistent results are obtained from the use of the starting plume constants.

An important and as yet unresolved problem is contained in the size spectrum of cumulus clouds. Typical radii range from 500 to 1500 meters Moreover, it has been observed that the tall cumulorimulus clouds are often found in an environment that is more stable than the environment containing a population of small cumulus clouds. Synoptic scale convergence patterns are apparently more important than the stability of the environment in determining the growth behavior of cumulus clouds.

POLLARD - Ocean currents from buoys

Data gathering in the ocean is much more difficult than in the atmosphere. Metal mooring lines tend to kink, while nylon lines in the North Atlantic are subject to "fish bite" (i.e. fish literally chew up the lines).

An area which has received considerable attention from the Words Hole Oceanographic Institution is known as site D, located at 39° 10'N 70°W which has a depth of 2600 meters. A schematic diagram of the energy spectrum appropriate for site D is shown below.

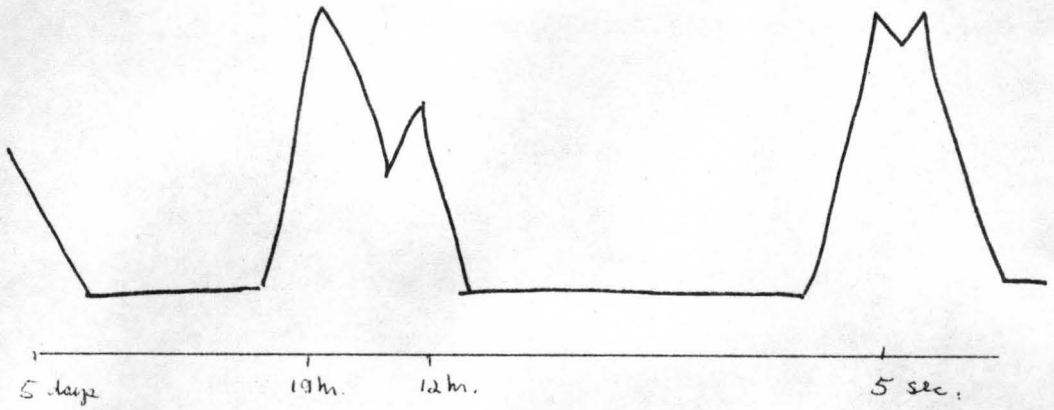

The peaks at 19 hours and 12 hours correspond to inertial and tidal oscillations, respectively. The primary interest lies in data of periods greater than one hour. The data have been gathered by sampling in rapid bursts. That is, every 15 minutes, the instrument turns on and measures every 5 seconds over a two minute interval.

MORTON - Limitations of similarity

Models such as the one-dimensional cumulus models may be termed "analog" models, as opposed "physical" models. If such an analog model contains a sufficient number of constants which may be determined from appropriate data, the model may be expected to give quite reasonable qualitative and quantitative predictions for the area in which it was developed. It is quite likely, however, that the model will fail miserably when conditions differ significantly from those conditions for which it was developed.

The similarity theory for a steady plume is not valid for heights less than 10 source diameters. Morton therefore concludes that such theories based upon a model of a plume should not be applied to cumulus clouds where the ratio of diameter to height is approximately three.

Morton believes that a cumulus cloud is not necessarily defined by its visible portion. Simpson, on the other hand, has observed "top hat" profiles of temperature and moisture which indicate that the visible cloud boundary and the actual cloud boundary are one and the same.

SIMPSON - Cumulus clouds and their transport

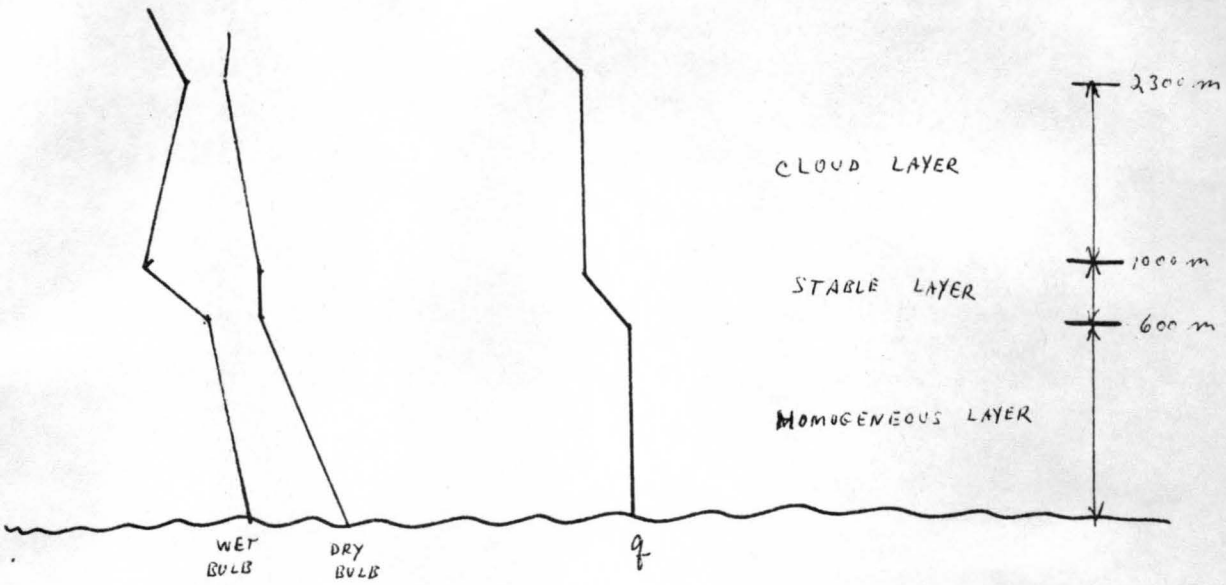

A mean schematic diagram of the trade wind boundary layer is shown above, where the boundary layer is defined as the layer in which the winds depart from their geostrophic values.

Cloud roots do not extend from the sea surface to cloud base. Positive vertical motions at cloud base are associated with positive

moisture anomolies, but the opposite is true of temperature fluctuations. Wind stirring is necessary to carry the moisture up to the condensation level.

Cumulus clouds are responsible for maintaining the downstream pressure gradients that maintain the trade wind regime against friction. The downstream balance of forces is a near balance between frictional forces and the pressure gradient force. The cross stream balance of forces is between the coriolis force and the pressure gradient force. A similar balance of forces occurs in some ocean boundary layers such as the Gulf Stream.

The trade winds export about 60% of the moisture that they pick up from the sea surface. In the sub cloud layer, eddies of the order 50 to 300 meters in diameter are responsible for the transfer of moisture up to cloud base. Trade wind cumuli then pump the moisture up through the cloud. If 94% of cloudy matter descends at a mean speed of 10 cm/sec, 6% of the cloudy matter need rise at a mean upward speed of 2 m/sec in order to carry out the necessary transports. The numbers given were derived from energy budget calculations and are in agreement with available observational evidence.

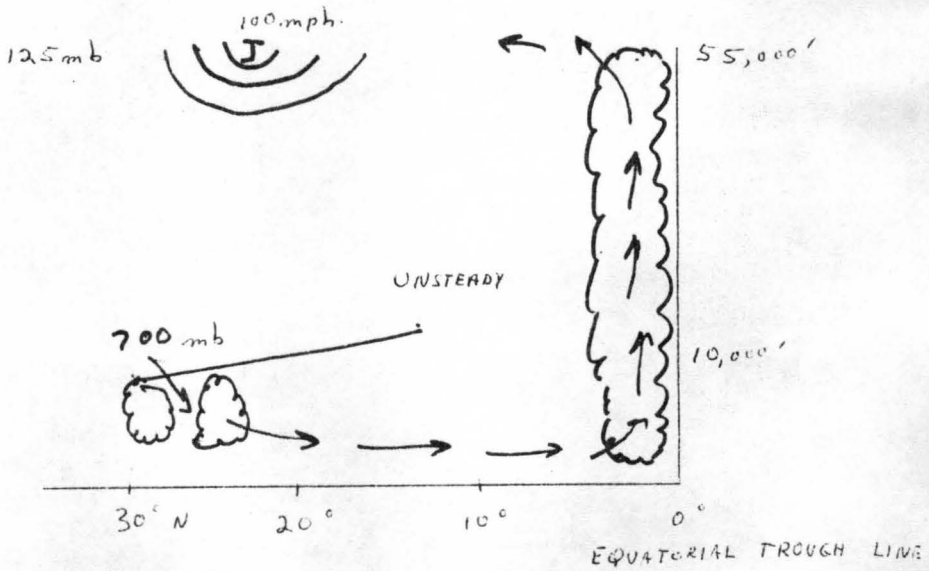

A schematic diagram of the zonally averaged equatorial zone is shown above. There is no heat flow across the equatorial trough line, although there is across the geographical equator. The rising portions of the Hadley cell are confined to restricted regions of active "hot towers" in which undilute sub-cloud air is pumped to great heights. Only 1500 to 5000 "hot towers" need to exist, on an average, in order to complete the energy balance requirements.

NAMIAS - Large scale air-sea interaction

Air-sea interactions are complicated by the fact that the two systems have different time constants. Sea temperature anomolies may last for a year or so and have a considerable effect on atmospheric circulations.

Let us consider for example a situation in which a third of the North Pacific somehow obtained a substantial positive temperature anomoly. If the warm pool results in more convection and cyclonic activity on the synoptic scale, radiation losses to space would be decreased, as well as evaporation losses from the sea. The longevity of the pool of warm water may therefore be increased to a year or longer.

Sub surface layers and mixing may be very important in influencing later events in the atmosphere. Strong winds associated with synoptic disturbances lead to an increased mixing to deeper depths in the ocean, thereby bringing deep temperature anomolies to the surface.

MORTON - Cloud models

J. Warner has doubts regarding temperature measurements in clouds, since the temperature excess of a cloud over its environment is usually of the order of half a degree. Conclusions drawn from temperature measurements in cloud may therefore be highly suspect.

Observations in Australia seem to indicate an increase of turbulence with height, which effect is exactly opposite to the observations of Simpson.

Warner observed poor average vertical continuity of updrafts in his clouds. The RMS vertical velocity increases with height according to the relation, $w = 1.2 + .72$, where z is measured in kilometers. Observations also indicate that the scale of turbulence is largest in the middle of the cloud and smallest at the bottom and top of the cloud.

According to Squires, some air in the center of clouds comes from above the cloud. This phenomenon cannot be taken into account by a steady state marching scheme which begins at the bottom of the cloud.

TURNER - Entrainment in stably stratified fluids

A plume immersed in a closed box in an initially unstable environment will lift warm air from the bottom of the box and eventually stabilize the environment. The effect of the plume on the environment can be examined if one adds to the entrainment equations,

$$-R^2 U = b^2 W \tag{148}$$

$$\frac{\partial \Delta_o}{\partial t} = -U \frac{\partial \Delta_o}{\partial z} \,, \tag{149}$$

where $\Delta_o = [g(\frac{\rho - \rho_o}{\rho_o})]$, U is the environment velocity, and R the radius of the box. The velocity may be shown to be proportional to the entrainment constant to the 4/3 power, and hence may be used to measure entrainment.

Although the problem is a time dependent problem, there is an asymptotic state. If Δ_o changes linearly in time,

$$G = \frac{-\partial \Delta_0}{\partial z} \propto F_0^{2/3} \alpha^{-4/3} H^{-8/3} f'\left(\frac{z}{H}\right), \tag{150}$$

where H is the height of the box.

Entrainment processes which have been considered so far have only involved horizontal processes, in which gravity plays no part. We will now consider vertical mixing, in which gravity enters into the problem.

Consider salt water flowing under fresh, where h represents the local depth.

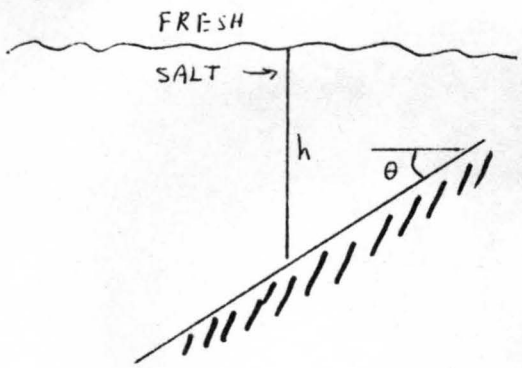

The conservation equations of mass and momentum may be written as

$$\frac{d(Uh)}{dx} = \alpha(Ri_0)U \tag{151}$$

$$\frac{d(U^2h)}{dx} = \Delta h \sin\theta - cU^2, \tag{152}$$

where the second term on the right represents an attempt to incorporate bottom friction.

$$Ri_0 = \frac{\Delta h \cos\theta}{U^2} \tag{153}$$

$$\Delta = g\frac{(\rho-\rho_0)}{\rho_0} \quad . \tag{154}$$

For the case when the bottom is not important (i.e., steep slopes), the velocity, U , is a constant, and $\frac{dh}{dx} = \alpha(Ri_o)$. The equations then give

$$\alpha = Ri_o \tan\theta \quad . \tag{155}$$

Experiments have been performed in which a grid has been moved through the upper layer of water that has a linear stable density gradient.

From dimensional considerations the ratio of the entrainment velocity u_e, to the friction velocity u_* should depend upon the depth of the mixed layer, h; upon the reduced buoyancy, Δ; and upon u_*. Experimental results lead to an expression of the form

$$E = \frac{u_e}{u_*} = 2.5\, Ri_*^{-1} \quad , \tag{156}$$

where Ri_* is a Richardson number based upon h, u_* and Δ. This is equivalent to an energy argument which says that the rate of supply of kinetic energy is proportional to the rate of change of potential energy of the system.

$$\frac{d}{dt}\left(\text{POTENTIAL ENERGY}\right) = 1.25\,\rho\, u_*^3 \quad . \tag{157}$$

Measurements in the ocean by Stommel indicate that the factor 1.25 should be replaced by the factor 10.

Mixing rates across an interface produced by salt lead to the following results:

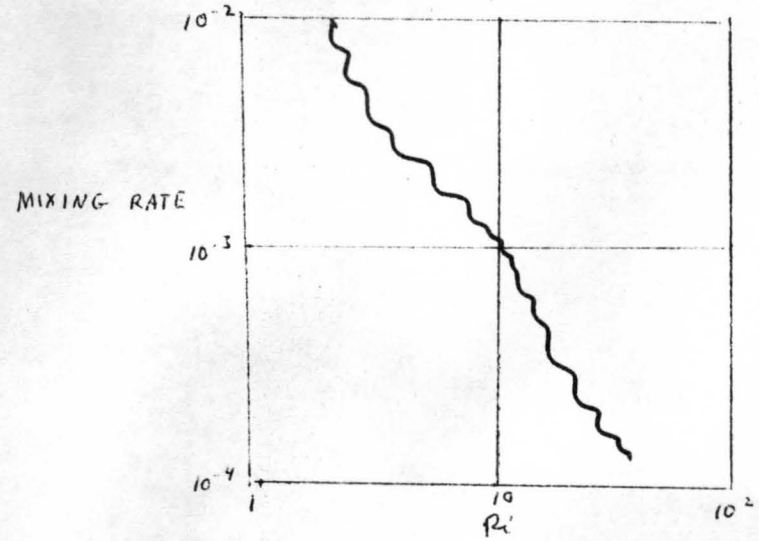

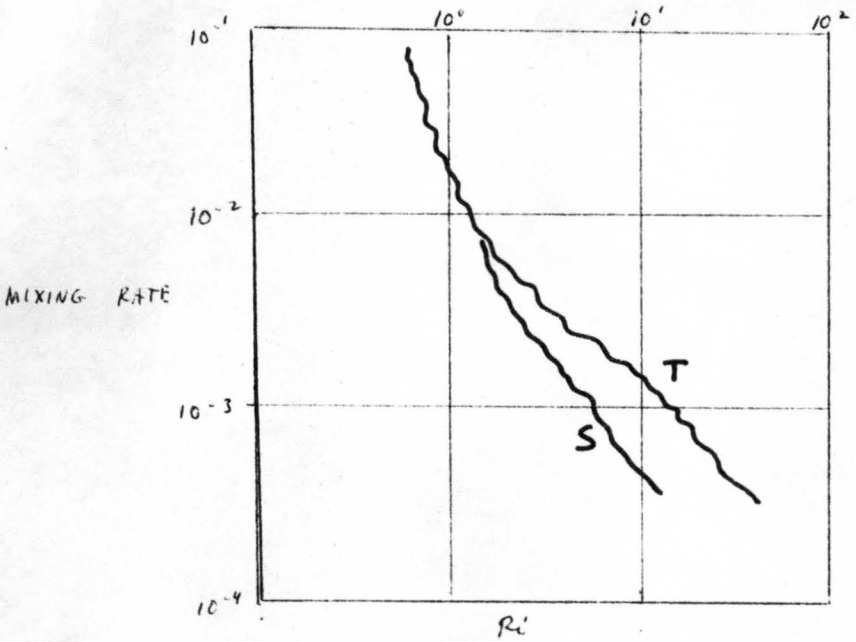

The curve denoted by T corresponds to interfaces associated with a temperature difference, while the curve denoted by s is associated with a salinity difference. These results indicate that heat diffuses faster than salt. If u_g represents the velocity of the grid,

$$\frac{u_e}{u_g} \propto Ri_o^{-1} \qquad (\text{HEAT}) \tag{158}$$

$$\frac{u_e}{u_g} \propto Ri_o^{-3/2} \qquad (\text{SALT}) \,, \tag{159}$$

where the velocity used in the definition of Ri_o is proportional to the grid frequency. Observations of Thompson lead to the result

$$\frac{d\overline{u^2}}{dz} \propto -\frac{\overline{u^2}}{\ell} \tag{160}$$

$$\frac{d\overline{u^2}}{dt} \propto \frac{u^3}{\ell} \,, \tag{161}$$

where ℓ represents the length scale of the turbulence.

TURNER - Thermocline development

The uppermost layers of the ocean may become homogenized through the action of the surface wind stress. An initially linear density gradient in the ocean would develop a surface layer of uniform density. The entrainment velocity of water into the surface layer would be proportional to the friction velocity, and inversely proportional to the Richardson number defined by $Ri_o = \dfrac{g\frac{\Delta\rho}{\rho}D}{u_*^2}$.

Let us now consider the simple case of a layer of fresh water surmounting a layer of salty water.

$$\frac{d}{dt}(\text{POTENTIAL ENERGY}) = \tfrac{1}{2}(g D \Delta\rho)\frac{dD}{dt} = \tfrac{1}{2} C u_e \,. \tag{162}$$

A constant entraining velocity u_e implies that the time change of potential energy is constant. For linear density gradients, the depth increases with time according to the relation

$$D(t) = u_* \left(\frac{15\,t}{N_o^2}\right)^{1/3} , \tag{163}$$

where $N_o^2 = \frac{g}{\rho}\frac{d\rho}{dz}$.

A time dependent model of the thermocline has been developed by Turner and Kraus. This one-dimensional model assumes: mechanical energy is constant; a periodic specific buoyancy flux; all the energy is used. The scaling parameters are then the rate of working by the stress ($\frac{g}{\rho} = u_*^3$), the maximum buoyancy flux (B_{max}), and the Period (P).

$$g\frac{\Delta\rho}{\rho} \propto \frac{B_{max}^2\, P}{G} \tag{164}$$

POLLARD - Inertial motions

Winds appear to be a major source of inertial motions in the ocean. Inertial oscillations may be likened to a simple pendulum, and are observed at all latitudes and at all depths. The periods vary from infinity at the equator to 24 hours at 30°N, and to 12 hours at the pole.

The data presented below indicate the magnitude and vertical distribution of inertial oscillations obtained during one observing period.

Depth (M)	10	50	100	500	1000	2000
Duration of record (days)	219	205	274	124	182	196
Max. amplitude (cm/sec)	49	20	14	13	11	7
amplitude which is exceeded only 10% of the time. (cm/sec)	23	9	8	9	4	3

The decrease in the amplitude of inertial oscillations with depth suggests the existence of a surface generation mechanism.

A simple time-dependent model has been developed to simulate the response of a homogeneous surface layer to a suddenly imposed wind stress. The predicted amplitude behavior is in fair agreement with observations. The equations that have been used are the following

$$\frac{\partial u}{\partial t} - fv = F - Cu \tag{165}$$

$$\frac{\partial v}{\partial t} + fu = G - Cv \,, \tag{166}$$

where

$$(F, G) = \frac{\rho_a C_D U^2}{\rho_w} (\sin\theta, \cos\theta) \,, \tag{167}$$

and where θ represents the angle between the surface wind and the coordinate axis. The second terms on the right side of the two time-dependent equations are really fudge factors which act as a dissipative mechanism to prevent an unreal energy build up.

SIMPSON - Cloud patterns

Satellite photographs show that the equatorial convergence zone exists on a day to day basis and not just on an average basis. These photographs also show many examples of cloud rolls as well as open and closed convection cells.

Laboratory convection studies may be of some value in obtaining a better understanding of the regular convection cells that appear in the atmosphere. There appears to be a paradox, however, in that the atmospheric

convection cells appear in a fully turbulent medium, whereas the laboratory convection cells do not.

Laboratory convection cells have the property that the fluid rises in the center of the cell and descends at the edge of the cell in liquids, but that the opposite pattern of vertical motion occurs in a gas. However, in rotating systems, the motion can be driven either way depending upon how fast the fluid is rotating. If you heat from below the central core will ascend, and if you cool from above, the central core will descend.

In non-rotating systems, the vertical motion patterns in liquids and gases may be attributed to the dependence of viscosity on temperature. In a gas, the viscosity increases with temperature and hence decreases upward in the convecting fluid, while in a liquid the viscosity decreases with temperature.

Atmospheric convection cells have width to depth ratio that is considerably larger than the laboratory cells. The vertical uniformity of the atmospheric cells in the presence of a wind shear suggests that the cells are confined primarily to the cloud layer and do not have roots extending down to the sea surface. Laboratory cells get stretched out into rolls. Open cells observed by satellites have a horizontal scale of about 75 km. Smaller cells on the order of 10 km have been photographed during manned space flights.

A major factor in the organization of cumulus clouds into organized lines is the wind shear. The fact that cloud lines are often organized along the direction of low level wind is due to the wind vector and wind shear vector being in the same vertical plane.

HADEEN - Numerical model of the boundary layer

A numerical model has been developed in order to obtain 24 hour forecasts for the continental U.S. Large scale 72 hour forecasts are used as boundary conditions for the local model. The layer of air between the surface and 1600 meters is divided into seven levels, and a 100 mile spacing is used between horizontal grid points. The level from the surface to the first level at 50 meters is taken to be a constant flux layer.

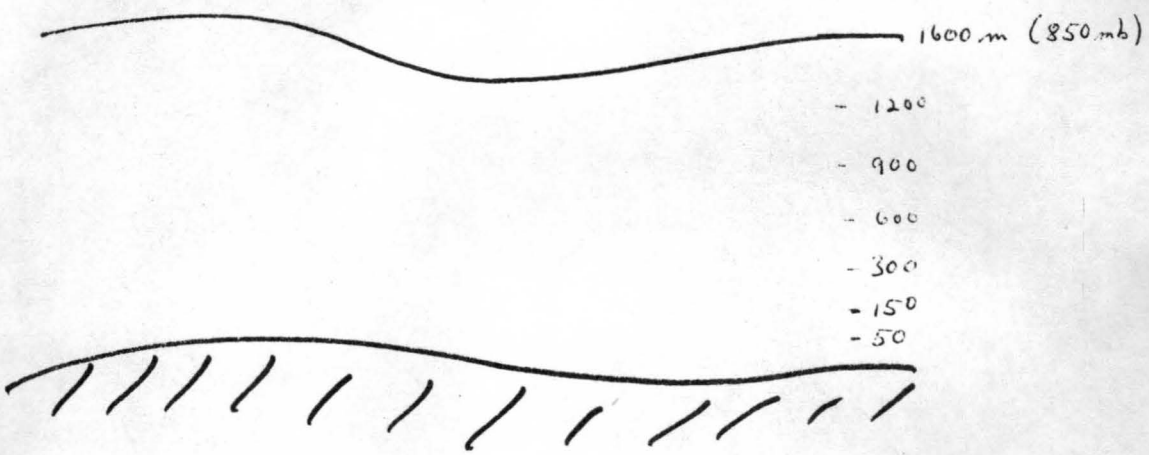

A model has also been developed for the European region, and one is currently being developed for an Asiatic region.

GARRETT - Generation of surface waves

The wind near the sea surface is often well approximated by a logarithmic profile, with the friction velocity being on the order of 3 to 4 percent of the wind speed at 10 meters. The input of momentum into the sea is very nearly equal to the surface stress.

All classical theories are inadequate to explain observed wave generation by at least an order of magnitude. Classical theories may be examined in light of the picture shown below.

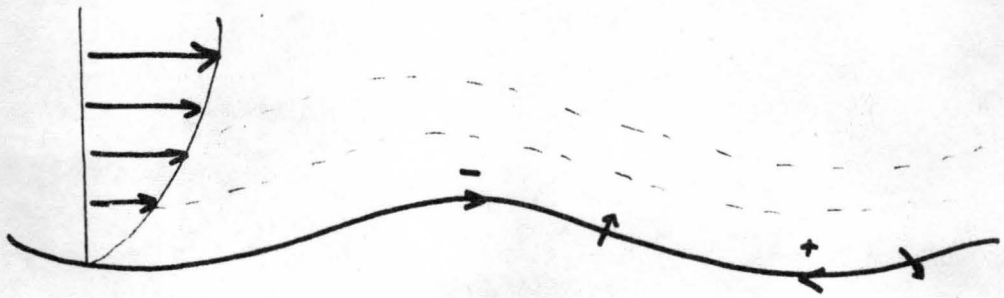

The signs refer to the pressure fluctuations. There is a coupling between pressure fluctuations and vertical velocities. Classical theories have attempted to shift the streamlines in order to permit the atmospheric pressure fluctuations to do some work on the sea surface.

A major deficiency of the theories (including the theory of Miles) is that they are formulated in terms of a single wave. This is a particularly unfortunate state of affairs because the largest wave is not the one that is growing most rapidly. Somehow, the energy input must be shifted into the lower frequencies.

A recent theory by Longuet-Higgens incorporates a coupling between the viscous stress and the horizontal velocities on the wave crests. Energy from the wind goes first into small waves, and then into large waves.

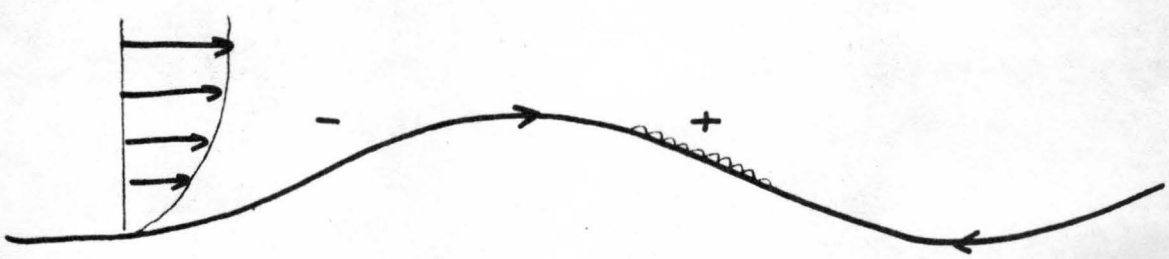

Some experiments by Dobson indicate that 80% to 100% of the wind stress goes into wave generation.

A fundamental difficulty may exist when one uses a wind tunnel to study wave generation. The laboratory experiment has a lid on the flow, and this upper boundary condition may invalidate a direct comparison between laboratory and field data if pressure gradients constitute an important part of the exchange process.

ELLISON - Dynamics of the atmospheric boundary layer

For about 50% of the time, there is a well mixed layer which is slightly stable in which the sea is warmer than the sea. For about 10% of the time there is a well mixed layer in which the air is stable with the air being warmer than the sea. The remaining 40% of the time may not be so easily classified. Moreover, it is clear that the density structure is much more important in boundary layer dynamics than the height of the Ekman layer.

There are four important mechanisms which may be responsible for the deepening of a boundary layer in an unstable regime. The first mechanism is convergence within the boundary layer. The other mechanisms which involve entrainment are as follows: turbulent mixing such as at the edge of a jet; surface heating, and resulting random fluctuations; evolution of thermals for the ratio of height to Monin-Obukhov length of order .3. An additional mechanism which may be important in connection with the evolution of thermals is the release of latent heat and the formation of clouds.

The Ekman spiral is determined by the eddy viscosity, but this is determined to a large extent by the density variations and not the

wind field. The integrated Ekman equations, however, may be of some use. For example the entrainment velocity at the top of the boundary layer may be obtained from the continuity equation.

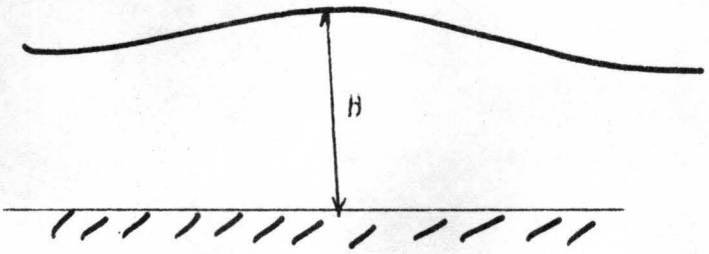

$$\frac{\partial H}{\partial t} + \frac{\partial}{\partial x}(H\hat{u}) + \frac{\partial}{\partial y}(H\hat{v}) = W_{Top}, \tag{168}$$

where the velocities are integrated values that are appropriate for the entire boundary layer.

Inertial oscillations occur in the atmosphere as well as in the ocean. These oscillations constitute an important mechanism in geostrophic adjustment processes.

POLLARD - Surface waves

A first order correction to the linearized theories may be obtained by considering a disturbance proportional to $e^{qz}\, e^{i(kx-\sigma t)/x'}$. The zeroth order solution may be written as

$$\underset{\sim}{u}_0 = a\sigma e^{qz}\left(\frac{q}{k}\cos x', \frac{q}{k}\frac{f}{\sigma}\sin x', \sin x'\right) \equiv \underset{\sim}{u} \tag{169}$$

the first order correction is

$$\underset{\sim}{u}_1 = \left(a^2\sigma\frac{q^2}{k}e^{2qz}, 0, 0\right) \equiv -\underset{\sim}{u}_s, \tag{170}$$

which may be identified as the Stokes drift.

The Eulerian and Lagrangian velocities in the rotating case are

$$\underset{\sim}{u}_E = \underset{\sim}{u} - \underset{\sim}{u}_S \tag{171}$$

$$\underset{\sim}{u}_L = \underset{\sim}{u} \; . \tag{172}$$

In the non-rotating case the velocities are

$$\underset{\sim}{u}_E = \underset{\sim}{u} \tag{173}$$

$$\underset{\sim}{u}_L = \underset{\sim}{u} + \underset{\sim}{u}_S \tag{174}$$

The singularity associated with the Coriolis parameter, f, going to zero can be gotten around by adding the homogeneous solution corresponding to inertial oscillations.

TURNER - Thermohaline layers

Most of the preceeding lectures have been concerned with high Reynolds number flows in which viscosity and thermal diffusivity are assumed to be relatively unimportant. However, molecular effects may be non-negligible in some cases.

The stratification in the ocean is not smooth, and R. Stuart thinks steps or discontinuities are to be expected in stably stratified fluids. ' may be expected to inhibit vertical mixing.

In the case of a fluid heated from below and which has a stable salinity gradient, overturning will occur in steps. Salt fingers, which

occur when salt is added at the top of a stable temperature gradient, are a phenomena which may be attributed to the more rapid horizontal diffusion of heat than salt.

Some concepts of high Rayleigh number thermal convection may be extended to a thermohaline or dual property system (i.e., it is assumed that the $Ra^{1/3}$ law holds). These predictions, which are born out by experiments are as follows:

$$FLUX = C\,(\Delta T)^{4/3} \tag{175}$$

where the constant c depends upon the two diffusivities, and is a slow function of $(\beta\Delta x/\alpha\Delta T)$.

Another important result is that the ratio of the fluxes is constant over a wide range of $(\beta\Delta x/\alpha\Delta T)$. For hot salty water above cold fresh water, the ratio is .56. For sugar-salt fingers the ratio is .9. For cold fresh water above hot salty water, the ratio is 0.15.

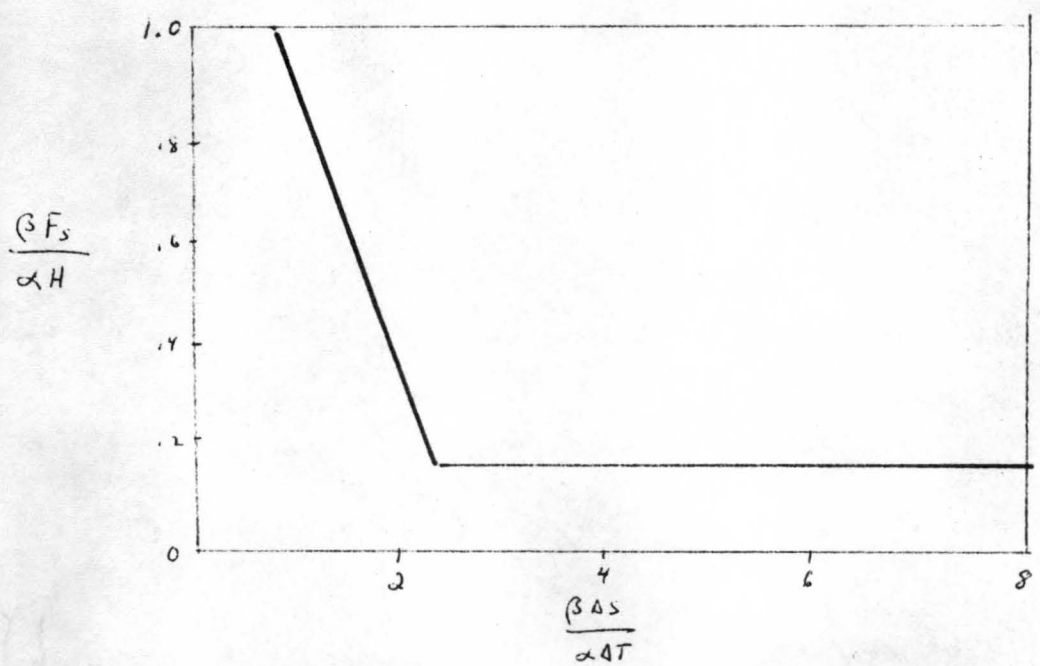

For a fluid of given properties and in the high Rayleigh number limit, the flux will depend upon ΔT and Δs. However the rate at which the flux dilutes will depend on the depth. Properties will change more rapidly in a shallow layer than in a deep layer.

Sloping boundaries result in special effects, and large scale motions may be set up.

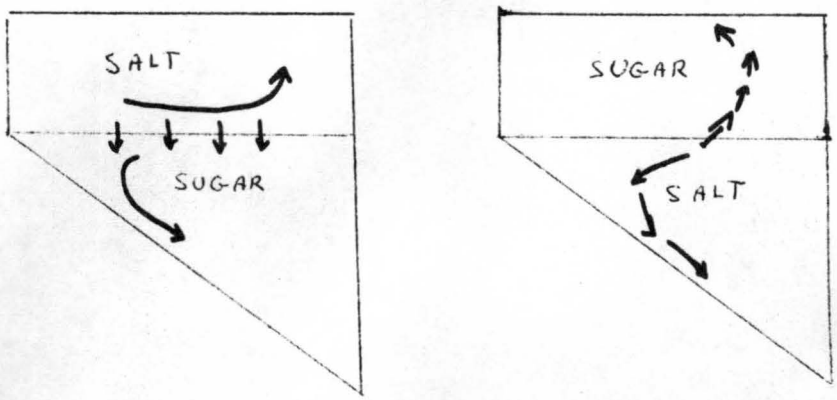

Shear effects associated with stirring are presently being studied by Linden, at Cambridge, England.

A technique has been developed to assist in the visualization of density gradients in two directions

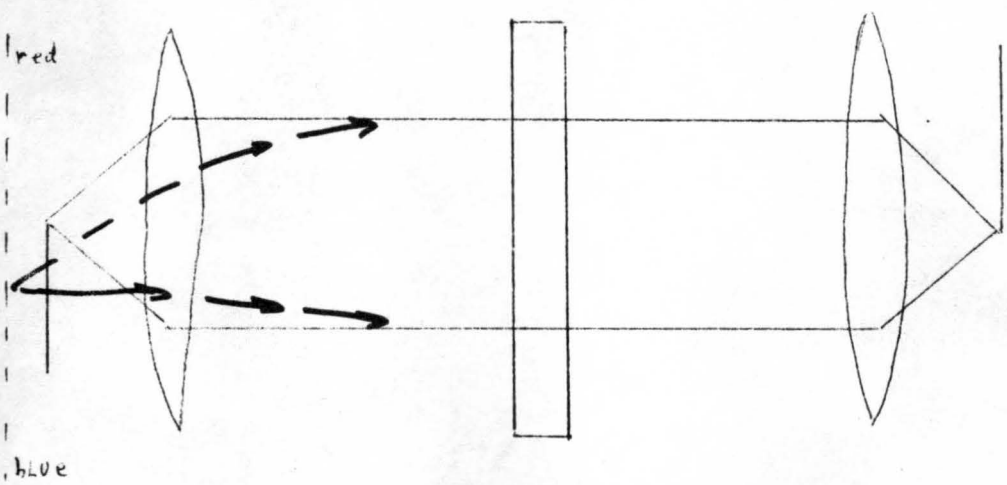

The ordinary Schlieren knife edge is replaced by a filter with red on top, blue on the bottom, and yellow on one side. Changes in density affect the path of light rays. Blue corresponds to a stable gradient and red an unstable density gradient. Horizontal density gradients will be indicated by the yellow coloring.

NAMIAS - Sea surface temperature anomaly

Ratcliff and Murray	Q.J.R.M.S.	1969 or 70
S. Tabata	Royal Soc. of Canada	1965
J. Namias	J.G.R.	October 1970
"	New Journal of Oceanography	1971
	M.W.R., J.G.R., Tellus	1955-1970
	Science	1965
	Deep sea Research (Fuglister Vol.)	1965
W. Jacobs	J.G.R.	1967
Shroeder and Stommel	Prog. in Oceanography (Sears, ed.)	1968?

Sea surface temperature departures from normal may amount to 2^{o}-3^{o} F, and may last for several years, based upon a 45 year average. A sea surface temperature anomaly curve for a station located at 35^{o}N-170^{o}W is shown below.

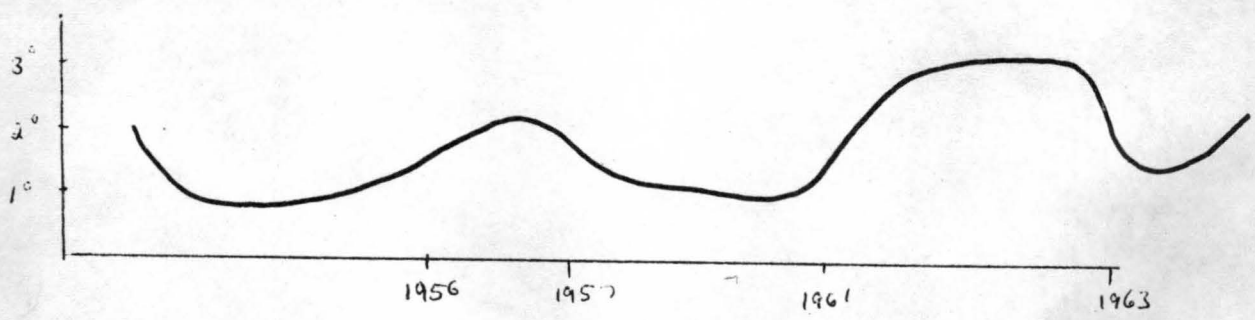

Temperature anomalies have been shown by Tabato to extend to depths of 500 meters.

Bjerknes has suggested that warm sea surface temperatures are associated with enhanced convective activity and precipitation. The occurrence of such warm temperature in the equatorial trough zone would be coincident with an increased Hadly circulation. The northward angular momentum transport is then variable, as is the strength of the mid-latitude westerlies.

There is significant correlation between sea surface temperature anomalies and sea level pressure.

ELLISON - Flow over mountains

Low hills as well as large hills can produce a large surface drag. Linearized lee wave theories are likely to do a bad job of estimating drag, since the conditions under which the theories apply are not very realistic. That is, the theories require that the hills be small.

Let us consider a stable, hydrostatic flow. The following two flow regimes are possible for flow over a two-dimensional hill,

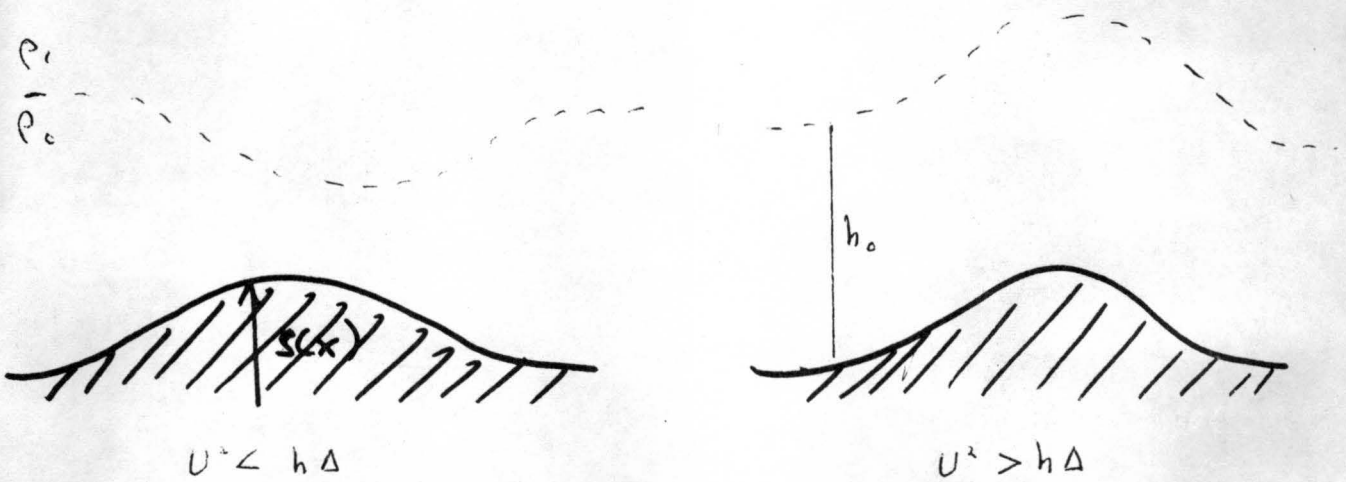

where $\Delta = g\Delta\rho/\rho$. If we define a Richardson number as $Ri_o = h\Delta/u^2$, there exists a critical value of $Ri_o = 1$, where the flow will not go over the hill. Simple minded theories won't get the flow over hills greater than about 200 meters.

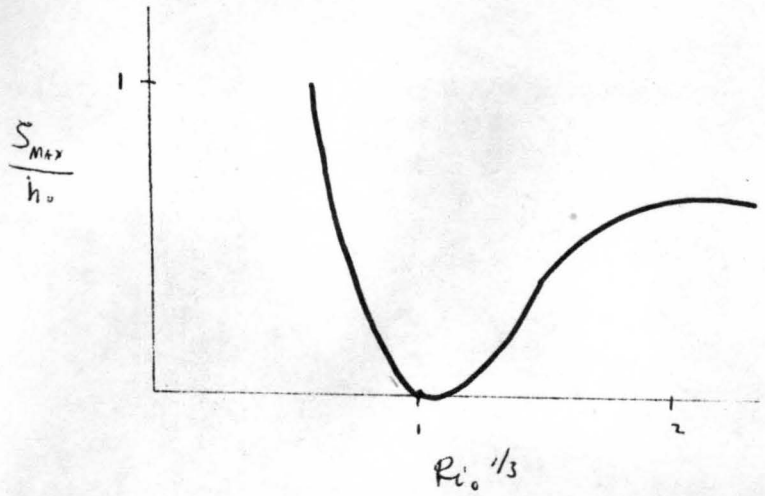

Drag will be enhanced if there is flow over a blocked layer such as is shown below.

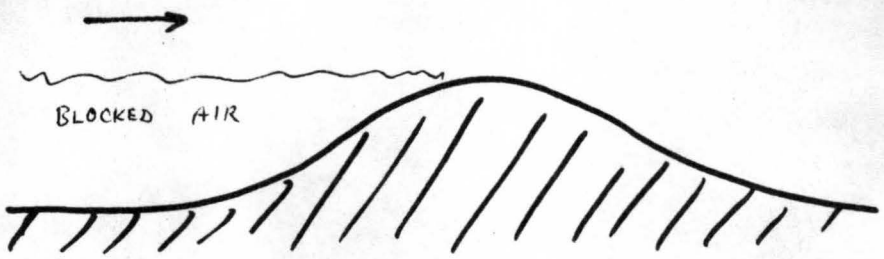

The atmospheric boundary layer should be treated as an entity in large scale numerical models. Only some gross features of the boundary layer should be incorporated into such models. However, one might use the integrated Ekman equations.

List of Participants

Belgium		
Van Hamme, J. L.	Belgium Roy. Met. Inst.	Maritime Meteorology
Brazil		
DeMesquita, A. R.	Southampton University	
Canada		
Garrett, J.	U.B.C.	Moored oceanographic buoy
Denman, K. L.	U.B.C.	Thermocline in relation to weather
Lozowski, E. P.	Toronto	Convection dynamics
Denmark		
Nielsen, A.	University Copenhagen	Wind on sea level
Busch, N. F.	Atomic Energy Commission	Atmospheric turbulence
Paulson, C. A.	Atomic Energy Commission	Atmospheric turbulence
Kristensen, L.	Atomic Energy Commission	Atmospheric turbulence
Larsen, S.	Atomic Energy Commission	Atmospheric turbulence
France		
Merlivat, Mrs. L.	French Atmoic Energy	Moisture flux by O^{18}
Saint-Guily, B.	Physical Oceanography Lab	Ocean boundary layer
D'Allonnes, R.	Physical Oceanography Lab	Ocean boundary layer
Germany		
Franz, H.	D.H.I.	Boundary layer over sea
Becker, G.	D.H.I.	Boundary layer over sea
Carlson, H.	D.H.I.	Boundary layer over sea
Wucknitz, J.	Hamburg University	Air-sea boundary layers
Prumm, D.	Hamburg University	Air-sea boundary layers
Krugermeyer, L.	Hamberg University	Air-sea boundary layers
Heinrich, M.	University of Kiel	Radioactive fluxes

Greece		
Frangos, A. C.	Space Research Center	Albedo
Iceland		
Karlson, T.	University of Iceland	Wind waves
Ireland		
O'Doherty, R.	University of Southampton	Marine meteorological spectra
Bates, J. R.	Irish Met. Service	Parameterization of b.l.
Italy		
Molcard	SACLANT	Ocean boundary layer
Netherlands		
Booy, R.	Tech. Univ. Delft	Research program
Oost, W. A.	K.N.M.I.	Air-sea interaction
Van der Kloet, P.	Tech. Univ. Delft	Research program
Norway		
Boyum, G.	Bergen University	Air-sea interaction
Dugstad, I.	Bergen University	Turbulent transport
Johanessen, O. M.	Bergen University	Ocean boundary layer
Portugal		
deCarvolho, M. M.	Nat. Civil Eng. Lab	Waves
Turkey		
Olcay, N.	Turkish Navy	Instruction
U.K.		
Killworth, P. D.	DAMPT Cambridge	Thermocline
Panter, R. J.	Admiralty Research Lab.	Small scale air-sea int.
Rayment, D. R.	Met. Office	Observation of atm. b.l.
Raddaway, R. W.	Univ. Edinburgh	Numerical models of b.l.
Thompson, N.	Met. Office	Observation from balloon

U.K. Continued

Whyte, K. W.	Met. Office	Numerical models
Edwards, Mrs. P.	N.I.O.	Observation of air-sea int.
Pitt, E. G.	N.I.O.	Spar buoy
Gash, J. H. C.	Institute of Hydrology	Evaporation
Taylor, P. K.	Univ. of Southampton	Observation of air-sea int.
Cattle, H.	Imperial College	Low latitude boundary layer
Morrision, G. K.	N.I.O.	Instrumentation of ocean h.l.
Gaunt, D. I.	N.I.O.	Oceanography
Pingree, R. D.	Univ. of Southampton	

U.S.A.

Pellissier, J. M.	Univ. of Miami	Hurricane
Smith, J. M.	Univ. of Miami	Numerical air-sea int.
Budgin, A. M.	Univ. of Miami	Acoustic radar
Berges, R.	U.C.L.A.	Air sea by chemical tracers
Lee, F. A.	Univ. Washington	Stratified flows
Green, T.	Univ. Wisconsin	Thermocline and waves
Wu, J.	Hydronautics, Inc.	Atmos. and Oceanic b.l.
Earle, M.D.	Oregon State Univ.	Waves and pressure fluctuation
Frenzen, P.	Argonne Nat. Lab.	Fluxes by buoy in BOMEX
Kroopnick, P.	Scripps	O^{18}/O^{16} in ocean
Colonell, J. M.	Univ. of Massachusetts	Sea surface dynamics
Gibson, C.	Scripps	FLIP and BOMEX
Nickerson, E. C.	Colorado State Univ.	Atmospheric boundary layer
Seaver, G. A.	Harvard	Turbulence in stratified fluid

Thompson, R.	Woods Hole	Thermocline model
Kreid, D. K.		
U. S. Air Force		
Stevens, D. W.	Aerospace Research (European Office)	Boundary layer
Hadeen, K.	Air Weather Service	Boundary layer models

The boundary layers of the atmosphere and ocean

Isle of Man, September 1970

Gravity waves - Introduction and elementary theory
(R. Dorrestein) - Abstract

1. Recommended textbooks.

O.M. Phillips, "The Dynamics of the Upper Ocean", 261 pp, Cambridge University Press, 1966 (very good account of the dynamics of surface waves and of the interactions, but concise).

B. Kinsman, "Wind Waves, their generation and propagation on the ocean surface", 676 pp, Prentice Hall, Inc., 1965 (also good but perhaps a little too copious).

H.H. Lamb, "Hydrodynamics" (Chapter IX: Surface waves, 113 pp), 6th Ed., Dover Publ., 1932 (a very good review of the "classical" works; does not use vector notation).

2. General.

Surface waves themselves, in deep water, can be considered as a boundary layer phenomenon, extending over a thickness of order K^{-1} (K is wave-number). Viscosity introduces effects in boundary layers which are much thinner.

Assumptions and limitations made:
- water incompressible, density constant;
- Coriolis acceleration neglected;
- influence of viscosity relatively small;
- minor consideration of:
  - surface tension and capillary waves,
  - atmospheric forces,
  - waves running to shore,
  - turbulence.

The two main aspects of wind waves and swell at sea are:
- some degree of periodicity;
- variability.

The latter can be divided into:
- stochastic variability - short-term and short-range (say within minutes or kilometres) and long-term;
- systematic variability - spatial and seasonal.

3. Basic dynamic equations.

Some simple relationships:
- surface slope and acceleration of surface particles,
- zero vorticity and non-zero mass transport.

4. Theory of purely periodic long-crested waves.

Simplest, but fairly useful, approximation: linearized (first order) theory. The dispersion law.

Theory of waves of finite height in deep water:

1. the fascinating, peculiar Gerstner wave,
2. the Stokes wave.

Vertical distribution of mass transport in these waves, in Eulerian or Lagrangian description.

5. Superposition of waves, group velocity.

Energy spectra:
one-dimensional, in terms of frequency or wave-number
two-dimensional, in terms of frequency and azimuth, or of wave-number space.

The boundary layers of the atmosphere and ocean

Isle of Man, September 1970

Observed characteristics of surface waves-spectra

(R. Dorrestein) - Abstract

Wind waves and swell. Fully developed seas.

1. Instrumental methods for observing waves:
   1. (most widely used). Record height variations of sea surface, along fixed mast or motion of floating object, as function of time.
   1a. Record height variations of sea surface and simultaneously slopes and perhaps curvatures of sea surface from the motions of a floating object, as function of time.
   1b. Record height variations of sea surface simultaneously at an array of probes at suitable distances, as function of time.
   2. Record wave profile at (approx.) one time.
   3. Apply stereophotogrammetry at one time.

2. Frequency distributions of "apparent" wave heights, wave periods and wave lengths. Empirical data. The Rayleigh distribution.

3. Introduction of spectra.

   In the definition and discussion of wave spectra, one mainly uses the concept of waves as a linear superposition of very many infinitesimal sine waves of various frequencies and wave-numbers and random phase (" Gaussian process").

   Method 1 above yields "time histories", from which one-dimensional frequency spectra may be computed.
   Methods 1a and 1b yield sets of signals, from which one-dimensional frequency spectra with additional information on direction spreading may be derived.
   Method 2 yields wave profiles, from which one-dimensional wave-number spectra may be computed.
   Method 3 yields instantaneous sea surface topography from which two-dimensional wave-number spectrum can be computed.

   One-dimensional spectra may be obtained, either by means of direct Fourier analysis and consequent grouping of squares of amplitudes, or by means of the covariance function and consequent Fourier transform. For two-dimensional spectra, only the latter procedure is feasible, for practical reasons.

   How is the relation between spectra and the distribution of "apparent" wave periods or wave lengths?

4. Discussion of spectra.

   General properties of observed frequency spectra of wind waves and of swell: normally one peak with a tail towards the higher frequencies*. Formula for the spectrum of a fully developed sea (Pierson and Moskowitz). Variability of spectra. Not so much information on directional spectra.* Discussion of this tail: the equilibrium range in which the spectrum $\phi(n) \sim n^{-5}$ (n is frequency.)

5. Other observed characteristics.
   Slope distributions. Orbital velocities. Number of white-caps. Short-

The boundary layers of the atmosphere and ocean

Isle of Man, September 1970

Transport of mass, momentum and energy in surface waves

(R. Dorrestein) - Abstract

Reference is made to Phillips' book "The Dynamics of the Upper Ocean", 1966, Chapter 3. For simplicity, the treatment is restricted here to two-dimensional (long-crested) waves.

. Irrotational waves on slowly varying uniform streams.

The equation for mass.
The equation for horizontal momentum: the waves are associated with an excess momentum flux or "radiation stress", which may give rise to variations in the mean water level. The balance of total energy in simplified form. Here again the "radiation stress" occurs.
Some consequences.

. Boundary layer effects.

Strictly virotational waves are not possible in anture. The free surface as well as the bottom (if the water is not very deep), by viscosity, necessarily introduce vorticity and some extra mass transport in the direction of wave propagation. These effects are mainly confined to boundary layers with thickness of order $\beta^{-1} = \sqrt{2\nu/\sigma}$ (ν is viscosity, $\sigma/2\pi$ is frequency), which is about 0,1 cm for waves of 1 second period.

M.S. Longuet-Higgins described these effects in a difficult article in 1953 but attention may be drawn to a simple physical picture of the effect at the bottom by the same author in a somewhat hidden appendix behind a paper of Russell and Osorio in Proc. 6th Conf. on Coastal Engineering (Council on Wave Research, 1958).

CHARACTERISTICS OF THE ATMOSPHERE BOUNDARY LAYER OVER THE SEA

Hans U. Roll
German Hydrographic Institute
Hamburg

REFERENCES:

ANIKIN, (1964): Trudy Morsk. Gidrofis. Inst. Akad. Nauk. SSSR 30, 35-40.

BLANCHARD, D.C. (1963): Progress in Oceanogr. 1, New York, Pergamon Press, 71-202.

BOUDREAU, R.D. (1964): J. Geophys. Res.

BROCKS, K. and L. Krügermeyer (1970): Berichte Inst. Radiomet. and Mar. Met. Hamburg, No. 14.

BUSINGER, J.A. (1966): Proc. Symp. Arctic Heat Budget, Atm.Circulation, RM-5233-NSF, Rand Corp., 305-

CHARNOCK, H. (1955): Quart. J. Roy. Met. Soc. 81, 639-640.

DARBYSHIRE, J. and M. (1955): Quart. J. Roy. Met. Soc. 81, 333-339.

DEACON, E. L. (1962): J. Geophys. Res. 67, 3167-3172.

DEACON, E.L. (1962): Proc. Symp. Math. Hydrodyn. Methods of Phys. Ocean., Hamburg, 385-398.

DEARDORFF, J.W. (1961): J. Geophys. Res. 66, 3613-3614.

DEARDORFF, J.W. (1968): J. Geophys. Res. 73, 2549-2557.

ELLISON, T.H. (1957): J. Fluid Mech. 2, 456-466.

FLEAGLE, R.G. and J.W. DEARDORFF, F.I. BADGLEY (1958): J. Marine Res. 17, 141-157.

HASSE, L. (1963): Tellus 15, 363-366.

HASSE, L. (1968): Hamburg. Geophys. Einzelschriften 11.

HÄUSSLER, W. (1955/56): Wiss. Z. Techn. Hochschule Dresden 5, 435-450.

HINZPETER, H. (1967): Meteor Forschungsergebnisse B No. 1, 41-44.

HOEBER, H.(1968): Tellus 30, 495-501.

JEFFREYS, H. (1925): Proc. Roy. Soc. (London) A 107, 189-206.

KARMAN, T.von (1934): J. Aeron. Sci. 1, 1-20.

KITAIGORODSKII, S.A. and Y. A. VOLKOV (1965): Izv. Atm. Ocean. Phys. Ser. I No. 9, 973-988.

KRAUS, E.B. (1966): J. Atm. Sci. 23, No. 4 443-445.

KRAUS, E.B. (1968): Bull. Amer. Met. Soc. 49, 247-253.

KOLMOGOROFF, A.N. (1941): C.R.Ac. Sci., USSR, 30, 301-

KUZNECOV, O.A. (1966): Akad. Nauk. SSSR, 78, 179-191.

MANDELBAUN, H. (1956): Trans. Amer. Geophys. Un. 37, 685-690.

McALISTER, E.D. and W. McLEISH (1969): J. Geophys. Res. 74, 3408-3414.

MILES, J.W. (1965): J. Fluid Mech. 22, 823-827.

MIYAKE, M., M. DONCLAN, G. McBEAN, C. PAULSON, F. BADGLEY and E. LEAVITT: Quart. J. Roy. Met. Soc. 96, 132-137 (1970).

MIYAKE, M., R.W. STEWART and R.W. BURLING (1970): Quart. J. Roy. Met. Soc. 96, 138-143.

MONOHAN, E.C. (1968): J. Geophys. Res. 73, 1127-1137.

MONIN, A.S. and A.M. OBUKHOV (1954): Trans. Inst. Geophys. Akad. Nauk SSSR 24, 151-

MUNK, W.H. (1947): J. Marine Res. 6, 203-218.

NAN-NITI, T., A. FUJIKI, and H. AKAMATSU (1968): J. Oceanogr. Soc. Japan 24, No. 6, 17-30.

NAN-NITI, T. (1969): Bull. Japanese Soc. Fish. Oceanogr. Special No. (Uda) 73-75.

OKUDA, S. and S. HAYAMI (1959): Records Ocean. Works Japan (NS) 5, 6-13.

OSHIVER, A.H. and G.A. BERBERIAN (1965): Geo. Marine Techn. 1, No. 4.

PANOFSKY, H.A. (1963): Quart. J. Roy. Met. Soc. 89, 85-94.

PAULSON, C.A. (1967): Sci Rept. NSF GP-2418, Dpt. Atm. Sci. Univ. Washington.

PHILLIPS, O.M. (1957): J. Fluid Mech. 2, 417-445.

PLATE, E. J. and G. M. HIDY (1967): J. Geophys. Res. 72, 4627-4641.

POND, S., R.W. STEWART and R.W. BURLING (1963): J. Atm. Sci. 20, 319-

POND, S., R.W. STEWART and R.W. BURLING (1966): J. Atm. Sci. 23, 376-386.

ROLL, H.U. (1948): Ann. Met. 1, 139-151.

ROLL, H.U. (1951): Ann. Met. 4, 269-286.

ROLL, H.U. (1965): Physics of the Marine Atmosphere, Intern. Geophys. Ser. 7, Acad. Press, New York.

RUGGLES, K.W. (1969): MIT, Dpt. Met. Report 69-1.

SAUNDERS, P.M. (1967): J. Atm. Sci. 24, 269-273.

SCHLICHTING, J. (1955): Boundary Layer Theory, McGraw-Hill, New York.

SCHOOLEY, A.H. (1967): J. Marine Res. 25, 60-68.

SHEPPARD, P.A. (1958): Quart. J. Roy. Met. Soc. 84, 205-224.

SMITH, S.D. (1967): J. Marine Res. 25, 239-262.

SMITH, S.D., L.A.E. DOE and R.G. STEVENS (1969): Atlantic Oceanogr. Lab., Bedford Inst., Rpt. 1969-5.

STEWART, R.W. (1961): J. Fluid Mech. 10, 189-194.

TAKAHASHI, T. (1958): Mem. Fac. Fish. Kagoshima Univ. 6, 1-46.

TAKEDA, A. (1963): J. Oceanogr. Soc. Japan 19, No. 3, 16-22.

VAN DORN, W.G. (1953): J. Marine Res. 12, 249-276.

WEILER, H.S. and R.W. BURLING (1967): J. Atm. Sci. 24, 653-664.

WILLIS, G.E. and C.A. PAULSON (1963): 1 Dpt. Atm. Sci. Univ. Washington, Annual Rpt. NSF, G 21575.

WU, J. (1968): J. Fluid Mech. 34, 91-122.

WU, J. (1969): J. Geophys. Res. 74, 444-455.

YEFIMOV, V.V. (1966): IInd Int. Oceanogr. Congress, Moscow, Abstracts 401-402.

ZILITINKEVICH, S.S. (1969): Tellus 21, 17-24.

ZUBKOVSKII, S.L. and T.K. KRAVCHENKO (1967): Izv. Atm. Oceanogr. Phys. 3, 73-77.

References for Lectures on Global Heat Budgets and

Synoptic-Scale Variations in Sea-Air Exchange

(Lectures I and II by J. Simpson)

Starred materials are considered the most important and highly recommended reading for the lectures.

I. General references on global heat budgets

*1. Malkus, J.S., 1962: Large-scale interactions. Chap. 4, The Sea: Ideas and Observations on Progress in the Study of the Seas. Interscience Publishers, New York and London, pp. 88-294.

2. Palmén, E. and C. W. Newton, 1969: Atmospheric circulation systems. Academic Press, New York and London, pp. 1-64.

3. Budyko, M.I., 1956: The heat balance of the earth's surface. Gidrometeorologicheskoe izdatel'stro, Leningrad, 255 pp. (Translated by Nina A. Stepanova; translation distributed by the U.S. Weather Bureau, Washington, D.C., 1958.)

4. Budyko, M. I., N. A. Epinova, L. I. Zubenok and L. A. Strokina, 1962: The heat balance of the earth's surface. Ak. nauk. U.S.S.R., Izv. ser. geograf., No. 1, pp. 6-16.

5. Sellers, W. D., 1965: Physical climatology. The University of Chicago Press, Chicago and London. Especially chapter 8.

II. Satellite papers bearing on energy budget computations

*6. Rasool, S. I. and C. Prabhakara, 1966: Heat budget of the southern hemisphere. In Problems of Atmospheric Circulation, Spartan Books, New York. pp. 76-92.

7. Fritz, S., P. Krishna Rao and M. Weinstein, 1964: Satellite measurements of reflected solar energy and the energy received at the ground. Jour. Atmos. Sci., 21, pp. 141-151.

8. Hanson, K. J., T. H. Vander Haar and V. E. Suomi, 1967: Reflection of sunlight to space and absorption by the earth and atmosphere over the United States during spring 1962. Monthly Wea. Rev., 95, pp. 354-362.

9. Winston, J. W., 1969: Global distribution of cloudiness and radiation as measured from weather satellites. Chap. 6, Climate of the free atmosphere, World Survey of Climatology, v. 4, Elsevier Publishing Co., Amsterdam.

10. Arking, A., 1964: Latitudinal distribution of cloud cover from TIROS III photographs. Science, 143, pp. 569-572.

III. Classical or important works on heat budget components

11. Jacobs, W. C., 1949: The energy acquired by the atmosphere over the oceans through condensation and through heating from the sea surface. J. Met., 6, pp. 266-272.

12. Jacobs, W. C., 1951: Large-scale aspects of energy transformations over the oceans. Compendium of Meteorology, Amer. Met. Soc., pp. 1050-1070.

13. London, J., 1957: A study of the atmospheric heat balance. N.Y. Univ., Dept Met. Oceanog. Final Rep., Project 131, Contract No. AF19(122)-165, 99 pp.

14. Houghton, H., 1954: On the annual heat balance of the northern hemisphere. J. Met., 11, 1-9.

15. Lumb, F. E., 1964: The influence of cloud on hourly amounts of total solar radiation at the sea surface. Quart. J. Roy. Met. Soc., 90, pp. 43-56.

*16. Colón, J., 1960: On the heat balance of the troposphere and water body of the Caribbean Sea. National Hurricane Research Project, Report No. 41. U.S. Dept of Commerce, Washington, D.C. 65 pp.

17. Starr, V. P., J. P. Peixoto and A. R. Crisi, 1965: Hemispheric water balance for the IGY. Tellus, 17, pp. 463-472.

IV References on heat transports by ocean currents

18. Bryan, Kirk, 1962: Measurements of meridional heat transport by ocean currents. Journ. Geophys. Res., 67 pp. 3403-3414.

*19. Emig, Marlies, 1967: Heat transport by ocean currents. Journ. Geophys. Res., 72, pp. 2519-2529.

20. Albrecht, F., 1960: Jahreskarten des Wärme- und Wasserhaushaltes der Ozeane, Ber. deut. Wetterdienstes, 66, Bd. 9, 19 pp.

V References on Synoptic-Scale Variations in Sea-Air Exchange

21. Malkus, J.S. and H. Riehl, 1960: On the dynamics and energy transformations in steady-state hurricanes. Tellus, 12, pp. 1-20.

22. Simpson, J., 1969: On some aspects of sea-air interaction in middle latitudes. Deep Sea Research, Supplement to vol. 16, pp. 233-261.

Also see pages 217-231 in reference 1.

References for Lectures on Cumulus Clouds, Their Role in Tropical Circulations and Cloud Patterns

(Lectures III, IV and V by J. Simpson)

I. Entrainment theory and observations; effects of wind shear

1. Stommel, H., 1947: Entrainment of air into a cumulus cloud. J. Meteor., 4, 91-94.

2. Malkus, J. S., 1954: Some results of a trade cumulus cloud investigation. J. Meteor., 11, 220-237.

3. Malkus, J. S., 1949: Effects of wind shear on some aspects of convection. Trans. Amer. Geophys. Un., 30, 19-25.

4. Malkus, J. S., 1952: The slopes of cumulus clouds in relation to external wind shear. Quart. J. Roy. Met. Soc., 78, 530-542.

II. Laboratory experiments on convection elements

5. Scorer, R. S. and C. Ronne, 1956: Experiments with convection bubbles. Weather, 11, 151-154.

6. Woodward, E. B., 1959: The motion in and around isolated thermals. Quart. J. Roy. Met. Soc., 85, 144-151.

7. Saunders, P. M., 1962: Penetrative convection in stably stratified fluids. Tellus, 14, 177-194.

8. Turner, J. S., 1962: The 'starting plume' in neutral surroundings. J. Fluid Mech., 13, 356-368.

III. Numerical cumulus models

9. Malkus, J. S. and G. Witt, 1959: The evolution of a convective element: A numerical calculation. The Atmosphere and the Sea in Motion. Rockefeller Institution Press, New York, 425-439.

10. Malkus, J. S., R. H. Simpson, D. A. Andrews and M. A. Eaton, 1965: Experimental cumulus dynamics. Reviews of Geophysics, 3, 387-431.

11. Murray, F. W. and C. E. Anderson, 1965: Numerical simulation of the evolution of cumulus towers. Douglas Report SM-49230, Douglas Missile and Space Systems Division, Santa Monica, California. 97 pp.

12. Murray, F. W., 1970: Numerical models of a tropical cumulus cloud with bilateral and axial symmetry. Monthly Weather Rev., 98, 14-28.

13. Lilly, D. K., 1962: On the numerical simulation of buoyant convection. Tellus, 14, 148-172.

14. Simpson, J. and V. Wiggert, 1969: Models of precipitating cumulus towers. Monthly Weather Rev., 97, 471-489.

15. Shafrir, U., S. Kaniel and B. Shkoller, 1970: Three-dimensional, time-dependent numerical experiments with dry and moist, shallow and deep convection models. Unpublished manuscript on file at Goddard Inst. for Space Studies, New York, 61 pp.

IV. Structure of the trade-wind boundary layer

16. Malkus, J. S., 1962: Large-scale interactions. Chap. 4. The Sea: Ideas and Observations on Progress in the Study of the Seas. Interscience Publishers, New York and London, pp. 88-294.

17. Bunker, A. F., B. Haurwitz, J. S. Malkus and H. Stommel, 1949: Vertical distribution of temperature and humidity over the Caribbean Sea. Papers Phys. Oceanog. Meteor., Mass. Inst. of Tech. and Woods Hole Oceanog. Inst., 11, 82 pp.

18. Malkus, J. S., 1958: On the structure of the trade-wind moist layer. Papers Phys. Oceanog. Meteor., Mass. Inst. of Tech. and Woods Hole Oceanog. Inst., 13, 47 pp.

V. Energetics and dynamics of Pacific trade-winds

19. Riehl, H., T. C. Yeh, J. S. Malkus and N. E. LaSeur, 1951: The north-east trade of the Pacific Ocean. Quart. J. Roy. Meteor. Soc., 77, 598-626.

20. Malkus, J. S., 1956: On the maintenance of the trade winds. Tellus, 8, 335-350.

21. Pike, A. C., 1968: A numerical study of tropical atmospheric circulations. Report of Contract No. F19628-68-C-0144. Inst. of Atmospheric Science, Univ. of Miami. 125 pp.

VI. Energetics and mechanisms of the equatorial trough zone

22. Riehl, H. and J. S. Malkus, 1958: On the heat balance in the equatorial trough zone. Geophysica (Helsinki), 6(3-4), 503-538.

See also Ref. 16, pp. 164-177 and Ref. 21.

VII. Cloud groups and patterns

23. Malkus, J. S. and H. Riehl, 1964: Cloud structure and distributions over the tropical Pacific Ocean. University of California Press, Berkeley and Los Angeles. 229 pp.

24. Bunker, A. F. and M. Chaffee, 1969: Tropical Indian Ocean Clouds. International Indian Ocean Expedition, Meteorological Monographs No. 4. East-West Center Press, Honolulu. 193 pp.

25. Malkus, J. S. and H. Riehl, 1964: Cloud structure and distributions over the tropical Pacific Ocean. Tellus, 16, 275-287.

26. Krueger, A. F. and S. Fritz, 1961: Cellular cloud patterns revealed by Tiros I. Tellus, 13, 1-7.

27. Kuettner, J., 1959: The band structure of the atmosphere. Tellus, 11, 267-294.

28. Avsec, D., 1939: Thermoconvective eddies in air. Application to Meteorology. Scientific and Tech. Pub. of Air Ministry Works of Inst. of Fluid Mech. of Fac. of Sci., Paris, No. 155. Published (in French) at Ed. Blondel la Rougery, 7, Rue St. Lazare, Paris.

29. Hubert, L. F., 1966: Mesoscale cellular convection. Meteorological Satellite Laboratory, Report No. 37. ESSA, U. S. Department of Commerce, Washington, D. C. 68 pp. (Has an excellent bibliography).

30. Simpson, R. H., N. Frank, D. Shideler and H. M. Johnson, 1968: Atlantic tropical disturbances, 1967. Monthly Weather Rev., 96, 251-259.

31. Baum, Robert A., 1970: The Eastern Pacific hurricane season of 1969. Monthly Weather Rev., 98, 280-292.

32. Malkus, J. S., C. Ronne and M. Chaffee, 1961: Cloud patterns in hurricane Daisy, 1958. Tellus, 13, 8-30.

33. Malkus, W. V. R., 1954: Discrete transitions in turbulent convection. Proc. Roy. Soc., A, 225, 185-195.

34. Malkus, J. S., 1955: The effects of a large island upon the trade-wind air stream. Quart. J. Roy. Met. Soc., 81, 538-550.

35. Malkus, J. S. and M. E. Stern, 1953: The flow of a stable atmosphere over a heated island, Part I. J. Meteor., 10, 30-41.

36. Stern, M. E. and J. S. Malkus, 1953: The flow of a stable atmosphere over a heated island, Part II. J. Meteor., 10, 105-120.

37. Smith, R. C., 1955: Theory of air flow over a heated land mass. Quart. J. Roy. Met. Soc., 81, 382-395.

CELLULAR CONVECTION

by

Prof. Dr. H. Siedentopf

(translation by Dr. Joanna Starr-Malkus and Mary C. Thayer)

Summary

The film shows the flows which arise upon the rearrangement of thermally unstable layers of gas or liquid in a gravitational field. The convection cells, which are steady or unsteady according to the experimental conditions, are shown from the top and in cross section.

The film is designed for college instruction. The narrow film (16 mm) silent version has a duration of 137 m or 12½ minutes at a projection speed of 24 B/s.

I. General Remarks

Convective motions are caused by local heating in gas and liquid layers found in a gravitational field. In the case of local temperature increase there comes about expansion and lowering of density of the gas or liquid element in question which thereby gains buoyancy relative to its surroundings. If the local heat source provides enough energy addition for maintenance, a steady convective flow builds up over the heat source. Such flows we find, for example, over a flame, a radiator and the like. Through the motions, heat energy from the warm source is transported into the surrounding medium, into which the flow, because of internal friction, spreads and mixes with the environment. If the energy supply is shut off, the flow quickly comes to a standstill.

1. Laminar and Turbulent Flows

However, each liquid or gas flow can occur in laminar or turbulent form; controlling the character of the flow is the Reynolds number

$$Re = \frac{\varrho \cdot v \cdot l}{\mu}$$

in which ϱ is the density, v the flow velocity, l the linear dimension, for example the diameter of the stream, and μ is the viscosity. According to kinetic theory of gases

$$\mu = \frac{1}{3} \varrho \cdot u \cdot \lambda ,$$

where u is the molecular velocity and λ is the mean free path of the molecule. The density therefore does not enter the dimensionless Reynolds number. If we designate $\mu/\varrho = \nu$ as the kinematic viscosity, the Reynolds number becomes

$$Re = \frac{v \cdot l}{\nu}$$

specified by the velocity and linear dimension of the flow and through a single material constant ν. Several values of the kinematic viscosity are here given:

Water	20°		$\nu = 0.010$ cm^2/s
Water	100°		$\nu = 0.0030$ cm^2/s
Glycerine	20°		$\nu = 6.8$ cm^2/s
Air	0°	and 760 mm	$\nu = 0.133$ cm^2/s
Air	100°	and 760 mm	$\nu = 0.245$ cm^2/s
Air	0°	and 760 mm	$\nu = 1.33$ cm^2/s

While for small Reynolds numbers, that is to say low velocities and dimensions, or large viscosity, the flow remains laminar and the individual stream filaments are parallel, at Reynolds numbers

greater than 1000 develops the eddying turbulent flow condition, in which the individual stream filaments cross each other and entangle. The division is not always sharp, which divides laminar from turbulent flow, as one can show through raising the velocity. It depends for example upon the strength of the effective disturbance.

The convective flow above a candle ($v \sim 20$ cm/s, $l = 1$ cm, $\nu = 0.3$ cm^2/s) is on account of Re ~ 70 surely laminar; over a larger surface, for example a hot plate ($v \sim 50$ cm/s, $l = 25$ cm, $\nu = 0.3$ cm^2/s) one obtains already Re $= 4.10^3$ and therefore turbulent eddying. Practically all fluid flows encountered in natural liquids (rivers, ocean currents) and gases (wind, flow processes in sun's atmosphere and stars) are, because of the large linear dimensions, turbulent, regardless of whether they have convective character or are brought into being by other forces. In the experiments shown in the film, the convective flows are laminar throughout because of their small scale.

2. Laboratory experiments on cellular convection

Under certain conditions the convective flows occur in a singularly regular form. If a horizontal liquid layer of large extent but small thickness - the experiment may be carried through in an exactly similar fashion with a gas layer - is heated from below, so arises an unstable condition, since the part of the layer near the bottom is warmer and therefore becomes less dense than the part near the upper surface. Ultimately therefore a rearrangement must take place, in which the hot portion rises from below

and the cold sinks from above. If one provides, through the continued heat source from below and heat sink at the top, for the maintenance of a temperature lapse in the layer, so continues the process of rising and sinking without limit. Therefore just as much fluid passes through each cross section in the middle moving upwards as downwards. If the layer thickness is on the order of 1 millimeter, the flow takes place in several stationary nearly equal-sized cells.

This cellular convection is easily demonstrated in the laboratory, by heating carefully oil, wax, or a similarly viscous substance in a shallow dish with even horizontal bottom, over an electric hotplate. The flow at the upper surface is made visible by the introduction of fine aluminum powder. (In the photographs paraffin liquid was used, which with adsorptive charcoal was colored black, in order to permit the motions near the surface to show up more clearly).

The cells are for the most part six-sided - still, four to seven-sided cells occasionally appear. The flow in the cells is naturally laminar because of the small dimensions and velocities. In the middle of the cells the fluid rises and it sinks at the edges. The rising occurs at higher speeds than the sinking; because of that the cross sections of the rising regions re smaller than those of the sinking regions.

In fully developed cellular convection the diameters of the individual cells are closely correlated with the layer thickness - they measure about $2\frac{1}{2}$ - $3\frac{1}{2}$ times the layer thickness. The nature

of the material is unimportant, also the temperature gradient has no significant influence on the proportionality factor. It makes no great difference whether the surface of the fluid freely borders on the air, or whether it is covered with a glass plate; in the second case it is difficult to keep down the fluid velocities of the individual cells - the cell size, however, only slowly changes The lifetime of the single cells is as large as desired, as long as the experimental conditions, temperature gradient and layer thickness remain constant.

If one investigates the influence of layer thickness on the convective flow more exactly, it appears that stationary cells only arise in a definite range of layer thicknesses. In the case of very thin layer thicknesses or very small temperature gradients, the onset of convection does not take place at all. The criterion for the onset of convection has been derived from the Navier-Stokes equations of motion of a fluid with friction by Rayleigh and Jeffreys. This can be expressed by the numerical value of a dimensionless constant, which we shall call the convection number

$$\lambda = \frac{dT}{dh} \cdot \frac{g \alpha c \varrho h^4}{k \nu}$$

in which dT/dh is the mean temperature gradient in the layer, g is the acceleration of gravity, α is the coefficient of expansion, c the specific heat, ϱ the density, h the layer thickness, k the thermal conductivity and ν is the kinematic viscosity. If the convection number exceeds a definite critical value, which depending on the boundary conditions falls between 700 - 1700, convection sets in and indeed in cellular form. For smaller values of λ the fluid remains at rest, the energy transport

resulting from the temperature difference is accomplished by molecular conduction. When the layer thickness is so large that the convection number attains a value of the order $\lambda = 10^{4.5}$ or greater, the character of the convective motions changes. Steady cells no longer form in one place, but individual fluid elements detach themselves from the bottom of the vessel, rise up and spread out upon the release of their heat content, at the upper surface. These ascents take place irregularly next to one another at different places in the fluid, so that we can speak of non-stationary convection. In the laboratory experiments with viscous fluids this situation begins with layer thicknesses greater than 15 - 20 mm. With in-between layer thicknesses we find a transition condition, next to the longer-existing cells non-stationary formations appear. Already in the case of layer thicknesses from about 8 - 10 mm up, the transition to unsteady convection begins to show up, in that occasionally division of old cells or new-formed cells occurs. In the unsteady flow condition, the life-duration of single cells has the magnitude of the layer thickness divided by the ascent velocity; the diameter of the cells is on the average about equal to the layer thickness, but the individual cells are often of very different sizes, since they exist side-by-side in different stages of development (see Fig. 3). In addition to changes in form and lifetime of individual cells, the changes in flow conditions with increasing convection number make themselves noticeable also in energy transport. The transition from pure conduction to cellular convection and cellular convection to unsteady convection can be

determined quantitatively fairly well, if one measures as a function of the convection number the heat transport between two horizontal plates placed over one another in a fluid (the lower plate is heated). Accordingly pure cellular convection is confined to a rather small range of λ ; it begins when $\lambda \succ 1700$, while the transition to unsteady convection occurs when $\lambda \succ 50{,}000$. This upper transition is relatively unsharp, since as already pointed out, a broad transition region exists, in which steady and non-steady cells appear side-by-side.

3. Convective processes in moving fluids

Also in a horizontally flowing fluid, which is made unstable by heating from below, can convection set in which superposes itself upon the basic motion. The patterns arising thereby are of very different kind, according to whether the velocity of the basic current or of the convection is greater. Moving cells can appear, which wander with the current but otherwise remain steady. Farther along it can come to the building of rolls, whose axes lie perpendicular to the direction of flow, and also rolls can build whose axes lie parallel to the direction of the flow. There arises in flowing destabilized gas layers, according to the boundary conditions, rolls parallel and perpendicular to the basic flow, as well as moving cells. In the earth's atmosphere, these processes are recognizable on a large scale in certain cloud structures.

4. Convection in the case of turbulent cell flow

In the discussion up to now it has been assumed that the flow in individual cells is laminar. When, as in nature it nearly

always is, the cells become so large, that the characteristic Reynold's number for the cell flow exceeds 10^3, the flow becomes turbulent. The convective phenomena which we encounter in nature, for example in the earth's atmosphere or the surface of the sun, are always of this kind. Also in the case of turbulent flow we can distinguish the two cases of cellular and unsteady convection. The convection number λ^* determining the transition takes a quite different form, since the coefficients of molecular conduction and internal friction are replaced by the corresponding turbulent Austausch coefficients (in general many orders of magnitude larger). We obtain for large-scale convection in gases

$$\lambda^* = \frac{d\theta}{dh} \cdot \frac{g\alpha h^4}{l'^2 u'^2},$$

where l' is the mixing length or diameter of the turbulent elements, u' is the mean velocity of the turbulent motions superposed upon the mean motions, and $\frac{d\theta}{dh}$ is the gradient of potential temperature, which takes into account the decrease of pressure with height. The critical values of the convection number are approximately the same as in the case of laminar convection.

5. Convection in the earth's atmosphere and surface of the sun

Examples of convective processes in the earth's atmosphere are visible in cloud formations, since rising air streams reach condensation by adiabatic cooling and thereby clouds are formed, while the surrounding regions of descent are cloud free. The case of unsteady convection we find realized in so-called "thermals", the convective motions which are brought about in strong sunshine by heating and thereby destabilizing the lowest air layer. If the

rising air is cooled by adiabatic cooling to the dewpoint temperature, which customarily occurs at a height of about 1000 m, so occurs condensation of water vapor and the building of fair weather cumulus clouds (see for example the cloud film "Cumulus Clouds"). The individual thermals have, as can be learned through sail plane flights, only a limited lifetime: single masses of warm air detach themselves from the bottom surface and rise, until their buoyancy is used up and they are mixed up with their environment. We have therefore in the lowest convection layer a typical case of unsteady convection. If one computes the pertinent convection number λ^* one arrives at a value the order of magnitude of $10^6 - 10^7$, therefore in any case well into the unsteady range. The diameters of the rising regions are in general smaller or at the maximum of the same magnitude as the layer thickness; also in this respect showing the proportions of the laboratory experiments. Since the cross section of the ascending regions is substantially smaller than that of the descending regions, the velocities of the updrafts are greater than the downdrafts. They measured about 1 - 3 m/s below small clouds and can in thunderclouds (cumulonimbus) rise to 10 m/s and higher; the downward velocities remain always below 1 m/s.

Stationary convection cells are also found frequently in the atmosphere; the corresponding cloud forms are the strato-cumulus in the lower atmosphere and alto-cumulus and cirro-cumulus clouds in the higher air layers (see Fig.4). The layer thicknesses are of the order of 100 m, the ratio of the cell diameter to the layer

thickness measures about 3.5. Values from 10^3 - 10^4 are obtained for the appropriate convection numbers. In fact it also appears that the single cells have a long lifetime. Since one is in the neighborhood of the lower critical boundary of the convection number, it is further understandable that, for example, stratocumulus elements often break out through a uniform stratus layer. A small variation of the layer thickness or the temperature gradient suffices to carry over the layer from the stable to the cellular convective regime.

Since the application of the laboratory results and calculations upon laminar convection to large-scale turbulent conditions in the earth's atmosphere leads to reasonable results, the further step to the sun's atmosphere appears justified. Although here the thermodynamic processes are much more complicated and besides the flow no longer incompressible, still in principle the process remains the same. We have known for a long time that under the photosphere of the sun there is a layer rendered unstable by the ionization of hydrogen which is at least 1000 km thick. The convection brought about thereby, causes irregular zones of uneven brightness on the sun's surface, which is designated as granulation. The regions of rising flow appear brighter than the in-between regions in which material slowly sinks. For the convection number we get roughly from a very uncertain calculation a value of about 10^7, so that we have to expect the case of unsteady convection. In fact the observations show that the diameter of the granules is the same order of magnitude as the layer thickness and further it can be established that the granules have a limited lifetime

of several minutes. Photographs at ten minute intervals show already significant differences. Calculation for the ratio of the layer thickness to the ascent velocity gives values of several minutes.

Similarly to the case of the sun, convective processes may play an important role in the surfaces of other stars, for example in certain classes of variable stars. Further it is envisaged that deep within the sun and stars convective flows play a part in carrying the energy released by the convection to the surface.

II. Explanation of the film

Laminar and turbulent convective flow

First of all the laminar convective flow over two lighted pipes is shown, which extend into the picture diagonally. The cross section of the flow measures 3 - 4 mm^2, the Reynold's number is about 10.

We see then the turbulent eddying convective flow over an electric hot plate. The flow is made visible by smoke of smoky candles which were set on the hotplate. One can recognize in this way how already after a short time the individual stream filaments become entangled. In order to follow the details of the flow better the motions are shown slowed down by a factor of $2\frac{1}{2}$. The Reynold's number of the flow measured about 5000.

Cellular Convection (12)

Stationary cells in an unstable fluid layer

First the apparatus is shown with which the experiments to follow are performed.

The vessel has a lower surface of 30 x 40 cm; it can be levelled by three foot screws.

The bottom surface can be heated with warm water through an ultra-thermostat, so that a vertical temperature gradient is created in the paraffin layer which is located in the vessel. The Askania-Z-camera with which the photographs of the convective processes in the layer are obtained is vertically mounted on a tripod above the vessel. The illumination is obtained with a spot light lamp. In order not to warm the upper surface of the convective layer unnecessarily and thereby to diminish the temperature gradient, a tray with water flowing through is placed in front of the lamp which in part absorbs its heat rays.

The next photograph shows a close-up of the convection vessel. The fluid is stirred around after being poured in, in order to create a completely random initial condition. From this initial condition now build up individual convection cells which in their grouping at first still show characteristics of the initial conditions. Gradually, however, a final condition is reached, with 5 - 7 sided cells all nearly the same size, and their positions and form no longer changes. This built-up steady end condition is in the case of small layer thickness (about 6 mm) once more shown in a photograph from the top.

The following photograph should make clear the development

of stationary cell flow in the individual members of a group. The flow is made visible in all photographs from the top through fine aluminum particles which are introduced in the paraffin which has been made dark by adsorption charcoal. The particles are carried along with the flow; they rise in the middle of the cells, move a short distance parallel to the surface and sink again at the edges of the cells.

Relation between layer thickness and cell diameter in a wedge-shaped layer.

In the case of the stationary end condition one recognizes the regular increase of cell diameter with layer thickness. Also it appears that the flow velocity in individual cells is larger, the larger the layer thickness and thereby the cells. On the left side, where the layer thickness becomes smaller than 1 mm, no more cells build, because here the critical value of the convection number is not attained.

Unsteady conditions in large layer thicknesses

In the case of moderately increased layer thickness the cell diameters are increased until the cells become no longer stable. Then if the layer thickness is further increased without however the cell diameter growing noticeably compared to its previous size, we find ourselves now in the transition region to unsteady conditions. The individual cells are less uniform than before and occasionally the division or formation of a cell takes place.

To make clear the formation and dissipation of individual cells in the case of unsteady convection, the next experiment was

taken in time-lapse (about ¼ the natural shutter-speed). In the next evenly heated layer there form after the onset of heating, convective currents which break through the upper surface. In consequence of the large layer thickness the formation of stationary cells does not occur but regularly new rising fluid forms which crowd out the old cells and in their turn have only a short existence. As a consequence of the time-lapsing, an actively boiling liquid is simulated through the building and dying cells.

Rolls and cells in a destabilized fluid current

In the photographs now following the fluid flows in a channel about 12 cm across, the bottom of which is warmed with an electric hotplate. The first photograph shows - after the onset of the heating - the building of rolls in the direction of flow, which further on break up into cells. In the case of smaller current velocities cells arise which wander with the current and remain for the rest unchanged.

Steady and unsteady convection cells seen from the side

The photographs in this group show the convective processes in a tray for side observation. Air serves as the medium: the flow is made visible through introduced cigarette smoke; the width of the tray measures 10 mm, the field of view shown in the photograph is about 12 cm in the vertical and 20 cm in the horizontal . The destabilization is brought about by a hot filament in the lower third of the tray. The tray is filled with cigarette smoke just above the top of the hot filament while the upper part contains pure air.

Cellular Convection (15)

After the onset of the heating there builds above the short spiral coil a local convection cell which becomes stationary after some time. In consequence of destabilization through a hot wire which is spread out across the length of the tray, so arises a great number of cells. In the case of weak heating the cells are nearly stationary. The currents do not reach the upper boundary of the tray. The thickness of the convective region is specified as follows: the energy released by the heat just balances that dissipated in the friction of the motions. In consequence of their inertia the currents penetrate some distance into the stable region below the hot wire. In the case of stronger heating steady cells no longer occur - the rising motion now lies here now there on the hot wire and there builds a complicated unsteady system in which the currents of the individual short-lived cells encroach upon one another.